

INVESTIGATION OF GROUNDWATER-SURFACE WATER INTERACTIONS AT  
SELECTED SITES ALONG THE RIO GRANDE USING HIGH FREQUENCY PRESSURE  
OBSERVATIONS

by  
Kimberly M. Bandy-Baldwin

Copyright by Kimberly Bandy-Baldwin 2012

All Rights Reserved

A thesis submitted to the Faculty and the Board of Trustees of the Colorado School of Mines in partial fulfillment of the requirements for the degree of Master of Science (Hydrology).

Golden, Colorado

Date: \_\_\_\_\_

Signed: \_\_\_\_\_  
Kimberly Bandy-Baldwin

Signed: \_\_\_\_\_  
Dr. Reed M. Maxwell  
Thesis Advisor

Golden, Colorado

Date: \_\_\_\_\_

Signed: \_\_\_\_\_  
Dr. David Benson  
Associate Professor and Program Director  
Hydrologic Science and Engineering

Signed: \_\_\_\_\_  
Dr. John Humphrey  
Professor and Head  
Department of Geology and Geological Engineering

## ABSTRACT

In the semi-arid southwestern United States, understanding the relationship between groundwater and surface water is important for sustainable water resources management. Albuquerque, NM, the largest population center in the state of New Mexico, obtains water from the Santa Fe Aquifer Group and the Rio Grande; therefore interaction between these two connected water resources is particularly important for local legislators and regulators. The United States Geologic Survey (USGS) established the Middle Rio Grande Valley Monitoring Network to better quantify water resources in this area. High frequency pressure, high frequency temperature, geologic coring, and slug test data were collected at eight locations in the Albuquerque, NM area from 2003 to 2010. These data and the fully-integrated, physical hydrology model, ParFlow were used to model the Barelás cross-section in order to better understand the system's response to perturbations in river stage. Thirty-six ParFlow models were created assuming three different subsurface scenarios: homogenous, layered and correlated, Gaussian random field. The domain extent, spatial discretization, total run time, and topography were kept consistent between all scenarios. Seven hydraulic conductivity values and three specific storage values were tested. All ParFlow models were spun-up to ensure steady state conditions and simulated for the 2006-2007 water year. Model outputs were compared to corresponding physically observed values to determine goodness of model fit and to assess any trends in the data. Hydraulic conductivity and specific storage were shown to play very different roles in the model predictions.

## TABLE OF CONTENTS

<b>ABSTRACT</b> .....	<b>III</b>
<b>LIST OF TABLES</b> .....	<b>VI</b>
<b>LIST OF FIGURES</b> .....	<b>ERROR! BOOKMARK NOT DEFINED.</b>
<b>ACKNOWLEDGMENTS</b> .....	<b>IX</b>
<b>CHAPTER 1: INTRODUCTION</b> .....	<b>1</b>
1.1 ANALYTICAL MODELS.....	2
1.1.1 Steady State Models.....	2
1.1.2 Transient Models.....	3
1.2 TRANSIENT ANALYTICAL MODEL - SHALLOW UNCONFINED FLOW WITH INFILTRATION.....	3
1.2.1 Horizontal Confined Flow.....	3
1.2.2 Horizontal Unconfined Flow.....	4
1.2.3 Shallow Unconfined Flow with Infiltration.....	5
1.3 NUMERICAL MODELS.....	6
1.3.1 ParFlow.....	7
1.4 HYDRAULIC RESIDENCE AND RESPONSE TIME.....	7
<b>CHAPTER 2: PURPOSE AND SCOPE</b> .....	<b>9</b>
<b>CHAPTER 3: STUDY AREA</b> .....	<b>10</b>
3.1 GEOLOGY.....	10
3.1.1 Rio Grande Rift and Middle Rio Grande Basin.....	10
3.1.2 Santa Fe Group and the Santa Fe Group Aquifer System.....	10
3.2 RIO GRANDE.....	12
3.3 CLIMATE.....	13
3.4 DESCRIPTION OF STUDY AREA.....	13
3.5 MIDDLE RIO GRANDE VALLEY MONITORING NETWORK.....	14
3.6 BARELAS CROSS-SECTION.....	17
<b>CHAPTER 4: METHODS</b> .....	<b>18</b>
4.1 DATA COLLECTION.....	18
4.1.1 Geologic Coring Data.....	18
4.1.2 High Frequency Pressure and Temperature Data.....	18
4.1.3 Slug Test Data.....	19
4.2 PARFLOW MODELS.....	19
4.2.1 Homogenous Model Simulations.....	21
4.2.2 Layered Subsurface Models.....	21
4.2.3 Random Field Models.....	24
<b>CHAPTER 5: GRAPHICAL ANALYSIS OF THE OBSERVED VALUES FOR THE BARELAS CROSS-SECTION</b> .....	<b>26</b>
<b>CHAPTER 6: DISCUSSION OF RIVER LEAKAGE FOR MIDDLE RIO GRANDE VALLEY MONITORING NETWORK</b> .....	<b>30</b>
<b>CHAPTER 7: ANALYTICAL MODEL RESULTS</b> .....	<b>32</b>
<b>CHAPTER 8: NUMERICAL MODEL RESULTS</b> .....	<b>34</b>
8.1 AVERAGE AND STANDARD DEVIATION.....	34
8.2 NUMERICAL MODEL SCENARIO COMPARISON PLOTS.....	42
8.3 OBSERVED VS. PREDICTED VALUES PLOTS.....	51
8.4 INDEX OF AGREEMENT.....	56
8.5 HYDRAULIC GRADIENTS.....	59
8.6 FOURIER TRANSFORMS.....	60
<b>CHAPTER 9: DISCUSSION AND CONCLUSIONS</b> .....	<b>67</b>
<b>REFERENCES</b> .....	<b>71</b>

## LIST OF TABLES

Table 3.1: Description of piezometer nest names and locations .....	16
Table 4.1: Description of piezometers include in ParFlow models. ....	20
Table 4.2: Description of parameters used homogenous subsurface model scenarios. ....	22
Table 4.3: Description of parameters used for layered subsurface models.....	23
Table 4.3 Continued.....	24
Table 4.4: Description of parameters used in random field subsurface model scenarios. ....	25
Table 5.1: Average and standard deviation for the observed values (ft asl). ....	28
Table 6.1: Mean hydraulic conductivities estimated from slug tests, feet per day. ....	30
Table 6.2: Average horizontal hydraulic gradients (-). ....	31
Table 6.3: Darcy flux calculations, feet per day. ....	31
Table 7.1: Transient Analytical Model Averages .....	32
Table 7.2: Transient Analytical Model Standard Deviation .....	33
Table 7.3: Transient Analytic Models Index of Agreement .....	33
Table 8.1: Average and standard deviation values for the homogenous subsurface models, the shallow piezometer locations are shown in the table. ....	35
Table 8.2: Average and standard deviation values for the homogenous subsurface models, the mid piezometer locations are shown in the table. ....	36
Table 8.3: Average and standard deviation values for the homogenous subsurface model case, the deep piezometer locations are shown in the table. ....	37
Table 8.4: Average and standard deviation values for the layered subsurface model cases, the shallow piezometer locations are shown in the table. ....	38
Table 8.5: Average and standard deviation values for the layered subsurface models, the mid piezometer locations are shown in the table. ....	39
Table 8.6: Average and standard deviation values for the layered subsurface models, the deep piezometer locations are shown in the table. ....	40
Table 8.7: Average and standard deviation value for the Random Field subsurface models, the shallow piezometer locations are shown in the table. ....	41
Table 8.8: Average and standard deviation values for the random field subsurface models, the mid piezometer locations are shown in the table. ....	41
Table 8.9: Average and standard deviation values for the random field subsurface models, the deep piezometer locations are shown in the table.....	42
Table 8.10: Index of agreement values for the homogenous subsurface model scenarios. ....	57
Table 8.11: Index of agreement values for the layered subsurface models. ....	58
Table 8.12: Index of agreement values for the random field subsurface models.....	58
Table 8.13: Comparison of Numerical Model Horizontal Gradients.....	59
Table 8.14: Comparison of Numerical Model Vertical Gradients near Rio Grande.....	60

## LIST OF FIGURES

Figure 1.1: Schematic of confined flow (Stark,1989).....	4
Figure 1.2: Schematic of unconfined flow (Stark, 1989).....	5
Figure 1.3: Schematic on shallow unconfined flow with infiltration (Stark,1989).....	6
Figure 3.1: Generalized cross-section of the Albuquerque Basin (Russel, 2002).....	14
Figure 3.2: Middle Rio Grande Valley Monitoring Network (Rankin, 2011). ....	15
Figure 3.3: Plan view of the Barelvas cross-section (adapted from Rankin, 2011).....	16
Figure 4.1: Cross-section schematic of ParFlow model domain (not to scale).....	19
Figure 4.2: Homogenous subsurface model domain, (note: 225 times vertical exaggeration). ....	21
Figure 4.3: Layered subsurface model domain, (note: 225 times vertical exaggeration). ....	22
Figure 5.1: Water table elevation at the Barelvas Transect 1 Piezometers for a four-year duration. .....	27
Figure 5.2: Comparison of standard deviation and distance from piezometer to the river. ....	29
Figure 8.1: Comparison of four homogenous subsurface model scenarios, the shallow piezometer locations are shown in the figure. ....	43
Figure 8.2: Comparison of four homogenous subsurface model scenarios from April 2007 to June 2007, the shallow piezometer locations. ....	44
Figure 8.3: Comparison of four homogenous subsurface model from April to June 2007, the mid piezometer locations are shown in the figure.....	45
Figure 8.4: Comparison of four homogenous subsurface model scenarios for April to June 2007, the deep piezometer locations. ....	46
Figure 8.5: Comparison of four layered subsurface model scenario for April to June 2007, the shallow piezometer locations. ....	47
Figure 8.6: Comparison of four layered subsurface model scenario for April to June 2007, the mid piezometer locations. ....	48
Figure 8.7: Comparison of specific storage for 15 ft/hr bulk hydraulic conductivity homogenous subsurface models, the shallow piezometer locations.....	49
Figure 8.8: Comparison of specific storage for Case 1 layered subsurface models, the shallow piezometer locations. ....	50
Figure 8.9: Comparison of specific storage for random field subsurface models, the shallow piezometer locations. ....	51
Figure 8.10: Plot of predicted vs. observed values of water table elevation for 0.417 ft/hr homogenous subsurface model. ( $ss=3.048 \times 10^{-5} \text{ ft}^{-1}$ ) .....	52
Figure 8.11: Plot of predicted vs. observed values of water table elevation for 3.750 ft/hr homogenous subsurface model. ( $ss=3.048 \times 10^{-5} \text{ ft}^{-1}$ ) .....	53
Figure 8.12: Plot of predicted vs. observed values of water table elevation for 15 ft/hr homogenous subsurface model. ( $ss=3.048 \times 10^{-5} \text{ ft}^{-1}$ ).....	54
Figure 8.13: Plot of predicted vs. observed values of water table elevation for Case 1 layered subsurface model. ( $ss=3.048 \times 10^{-5} \text{ ft}^{-1}$ ).....	55
Figure 8.14: Plot of predicted vs. observed values of water table elevation for random field subsurface model. ( $ss=3.048 \times 10^{-5} \text{ ft}^{-1}$ ).....	56
Figure 8.15: Fourier transforms for the 0.417 ft/hr bulk hydraulic conductivity model. Shallow piezometer locations are shown here. ....	61
Figure 8.16: Fourier transforms for the 15ft/hr bulk hydraulic conductivity homogenous subsurface model. Shallow piezometer locations are shown here. ....	62
Figure 8.17: Fourier transforms for the 15ft/hr bulk hydraulic conductivity homogenous subsurface model. Mid piezometer locations are shown here.....	63

Figure 8.18: Fourier transforms for the 15 ft/hr bulk hydraulic conductivity homogenous subsurface model. Deep piezometer locations are shown here..... 64  
Figure 8.19: Fourier transforms for the Case 1 layered subsurface model. Shallow piezometer locations are shown here..... 65  
Figure 8.20: Fourier transforms for the random field subsurface model. Shallow piezometer locations shown here..... 66

## **ACKNOWLEDGMENTS**

I would like to express my deepest gratitude to those individuals who have helped and supported me throughout my project. I wish to thank my husband, William Baldwin; my mother, Sheri Johnson-Spader; my sister, Jessica Gershin; and my friend, Moran Stumb, for their unwavering devotion and encouragement. I am grateful to my advisor, Dr. Reed Maxwell, for his time and guidance throughout my project. I would like to thank the Club 124 research group, with a special thanks to Laura Condon, Erica Siirila, and John Williams, for their advice, ideas, revisions, and support.

## CHAPTER 1: INTRODUCTION

In the semi-arid southwestern United States sustainable water resources management requires an understanding of the relationship between groundwater and surface water. Many communities in the southwest are solely reliant on groundwater, but in areas where surface water is present, it is often used to augment groundwater for drinking water purposes. Albuquerque, NM, the largest population center in the state of New Mexico, obtains groundwater from the Santa Fe Aquifer Group and surface water from the Rio Grande River for its municipal supply. The city's dependence on both groundwater and surface water makes the characterization of interactions between these connected resources particularly important to local legislators and regulators. To better characterize the relationship between the Santa Fe Aquifer Group and the Rio Grande, the United States Geologic Survey (USGS) New Mexico Water Sciences Center in collaboration with the Middle Rio Grande Endangered Species Collaborative Program and the U.S. Army Corps of Engineers established the Middle Rio Grande Valley Monitoring Network. The USGS collected high frequency pressure, high frequency temperature, geologic coring, and slug test data at eight locations in the Albuquerque, NM area from 2003 to 2010. A physically based, fully integrated hydrologic model was utilized to investigate these interactions and sensitivity to a number of parameters.

Groundwater and surface water are coupled components of the hydrologic cycle, where the quantity and quality of the water are often considered interdependent (Spanoudaki, 2010; Sophocleous, 2002). Over the last sixty years, many analytical and numerical models have been developed to better understand and quantify the relationship between these related water sources (Butler, 2001; Christensen, 2009; DHI-WASY Software, 2012; Fetter, 2001; Harbaugh, 2000; Hunt, 1999; Maxwell, 2010; Kollet, 2003, 2007; Serrano, 1998; Spanoudaki, 2010; Strack, 1989). Models are generally developed for one or more of the following reasons: 1) to predict the results of a perturbation to the system, i.e., a contaminant spill or pumping of groundwater, 2) to better understand the relationship between model parameters, 3) to organize field data, and/or 4) to analyze flow in a hypothetical hydrogeologic systems (Anderson, 2002).

## 1.1 Analytical models

An analytical model is a closed form expression, which provides a single solution for a set of state variables. Analytical models are inexpensive to produce, easily and quickly solved, and often require less data collection than numerical models (Fetter, 2001). They can be applied to provide insight into the dependence of the solution on state variables, improve the understanding of physical processes occurring, and they provide a method to validate numerical model simulations (Spanoudaki, 2010). However, analytical models are limited by the requirement of a simplified homogenous isotropic domain and idealized boundary conditions (Fetter, 2010). Many analytical models have been developed to describe groundwater-surface water interactions (Butler, 2001; Christensen, 2009; Fetter, 2001; Hunt, 1999; Kollet, 2003, 2007; Serrano, 1998; Spanoudaki, 2010; Strack, 1989). These models can be split into two categories: steady-state models and transient models, as described below.

### 1.1.1 Steady State Models

A steady-state model is one that assumes the hydrologic system is in equilibrium. An example of a steady-state analytical model is Darcy's law. In 1865, Henry Darcy experimentally determined the equation for saturated fluid flow through a porous media, later known as Darcy's Law (Brutsaert, 2005). Darcy's Law is often expressed as:

$$Q = KA\nabla h \quad (2.1)$$

where  $Q$  is the flow rate ( $L^3T^{-1}$ ),  $K$  is the hydraulic conductivity ( $LT^{-1}$ ),  $A$  is the cross-sectional area ( $L^2$ ), and  $\nabla h$  is the hydraulic gradient operator (-) (Brutsaert, 2005; Dingman, 2002; Fetter, 2001). Darcy's law describes the flow at a "point", which is driven by the spatial hydraulic gradients (Dingman, 2002). The hydraulic gradient is expressed as:

$$\nabla h = \frac{h_1 - h_2}{L} \quad (2.2)$$

where  $h_1$  is the hydraulic head at location one (L),  $h_2$  is the hydraulic head a location two (L), and  $\Delta l$  is the length between location one and location two (L) (Fetter, 2001).

The Darcy flux ( $q$ ) represents saturated fluid flow per unit area of material. It can be derived from Darcy's Law by assuming the cross-sectional area and length become infinitesimally small and is expressed as:

$$q = -K\nabla h \quad (2.3)$$

where  $q$  is the Darcy flux and  $\nabla h$  is the hydraulic gradient operator (-) (Fetter, 2001). Hydraulic gradients are dependent fluid density and the pressure gradients.

### 1.1.2 Transient Models

A model that analyzes time-dependent problems is a transient model. Most transient models begin with steady-state initial conditions and produce a set of head values for each time step, thus showing changes in the hydrologic system with time (Anderson, 2002). Many transient, analytical models have been developed for groundwater-surface water interactions (Butler, 2001; Christensen, 2009; Fetter, 2001; Hunt, 1999; Kollet, 2003, 2007; Serrano, 1998; Spanoudaki, 2010; Strack, 1989).

## 1.2 Transient Analytical Model - Shallow Unconfined Flow with Infiltration

### 1.2.1 Horizontal Confined Flow

A horizontal confined flow model example is shown in Figure 1.1. This model example assumes that flow occurs in an aquifer between a fully penetrating river and a boundary. The  $x$  and  $y$  axes are normal and parallel to the river and the boundary, the  $z$ -axis points vertically upward, and the origin is in the center of the domain. The head at the river and the boundary are known and are represented by  $\phi_1$  and  $\phi_2$ , respectively. It is assumed that flow in  $y$  and  $z$  directions is negligible ( $q_y = q_z = 0$ ). The head at location  $x$  is expressed as:

$$\phi = -(\phi_1 - \phi_2) * \frac{x}{L} + \frac{1}{2} * (\phi_1 + \phi_2) \quad (2.4)$$

where  $\phi$  is the head at location  $x$  (L),  $x$  is the location of the piezometer (L), and  $L$  is the distance between the river and the boundary (L) (Strack, 1989).

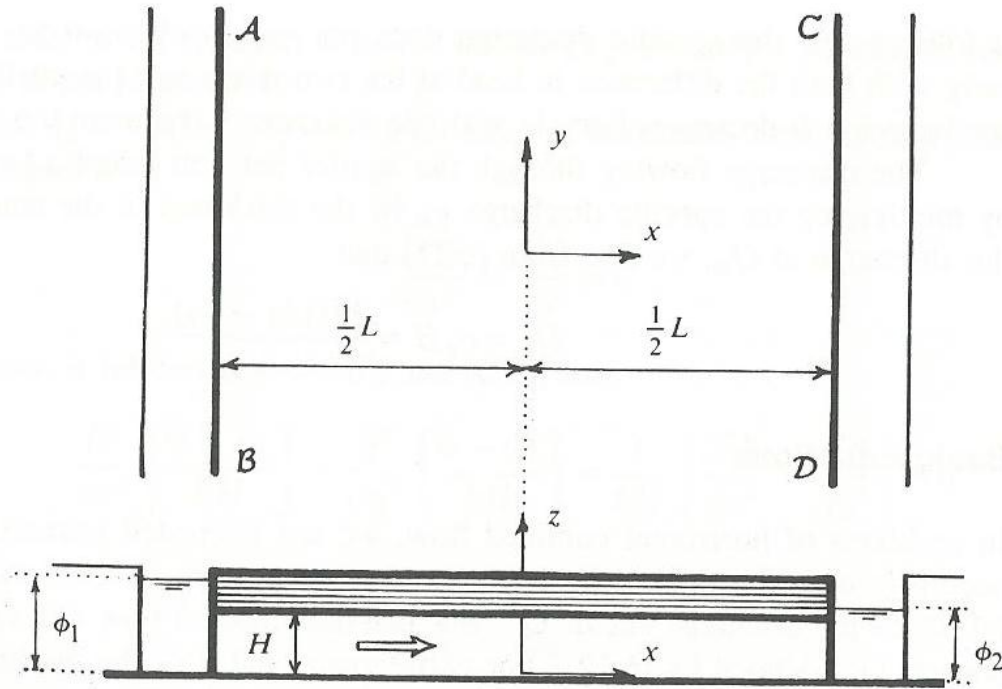


**Figure 1. 1: Schematic of confined flow (Stark,1989).**

### 1.2.2 Horizontal Unconfined Flow

A horizontal unconfined flow model example is shown in Figure 1.2. Similarly to the horizontal confined flow model, flow in for the horizontal unconfined flow occurs in an aquifer between a fully penetrating river and a boundary. The y axis is normal and parallel to the river and the boundary and the origin is in the center of the domain. The head at the river and the boundary are known and are represented by  $\phi_1$  and  $\phi_2$ , respectively. The head at location x is expressed as:

$$\phi = \sqrt{\frac{1}{2} * (\phi_1^2 + \phi_2^2) - \frac{\phi_1^2 - \phi_2^2}{L} * x} \quad (2.5)$$

where  $\phi$  is the head at location x (L), x is the location of the piezometer (L), and L is the distance between the river and the boundary (L) (Strack, 1989).

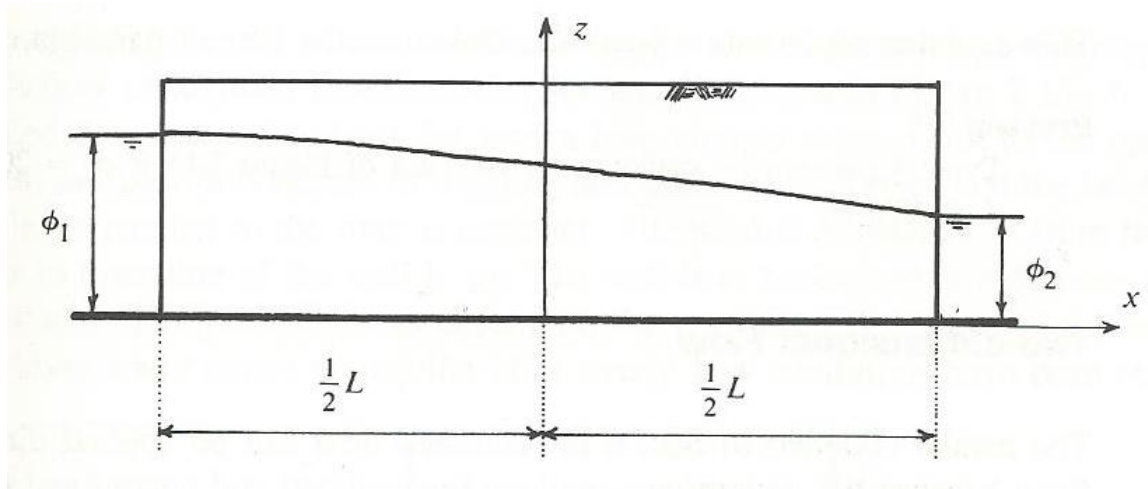


**Figure 1. 2: Schematic of unconfined flow (Stark, 1989)**

### 1.2.3 Shallow Unconfined Flow with Infiltration

An example of shallow unconfined flow model, which includes infiltration, is shown in Figure 1.3. This model assumes the river is partially penetrating. Therefore, the bottom of the river is not directly in contact with the phreatic surface. River water leaks through the streambed and infiltrates to the phreatic surface below. The head at the two boundaries and the infiltration rate from the river are known and are represented by  $\phi_1$ ,  $\phi_2$ , and  $N_1$ , respectively. The potential for flow at location  $x$  is expressed as:

$$\Phi = -\left(\frac{1}{2} * k * \phi_1\right) * \frac{x - \frac{1}{2}L}{L} + \left(\frac{1}{2} * k * \phi_2\right) * \frac{x + \frac{1}{2}L}{L} + N_1 * G_d(x, \epsilon_1, \epsilon_2) \quad (2.6)$$

where  $\Phi$  is the potential for flow at location  $x$  (L),  $k$  is the hydraulic conductivity (L/T),  $x$  is the location of the piezometer (L),  $L$  is the distance between the river and the boundary (L),  $G_d$  is the function that models the infiltration rate,  $\epsilon_1$  is the left boundary of the river, and  $\epsilon_2$  is the right boundary of the river.  $G_d$  at location is expressed as:

$$G_d(x, \epsilon_1, \epsilon_2) = aF_2 = \left[ \left(\frac{1}{2}L - \epsilon_2\right) b + \frac{1}{2}b^2 \right] \frac{x + \frac{1}{2}L}{L} \quad -\frac{1}{2}L \leq x \leq \epsilon_1 \quad (2.7)$$

$$G_d(x, \epsilon_1, \epsilon_2) = aF_2 - \frac{1}{2}(x - \epsilon_2)^2 \quad \epsilon_1 \leq x \leq \epsilon_2 \quad (2.8)$$

$$G_d(x, \varepsilon_1, \varepsilon_2) = aF_2 - b(x - \varepsilon_2) - \frac{1}{2}b^2 \quad \varepsilon_2 \leq x \leq \frac{1}{2}L \quad (2.9)$$

The head at location  $x$  is expressed as:

$$\phi = \sqrt{\frac{2\Phi}{k}} \quad (2.10)$$

(Strack, 1989).

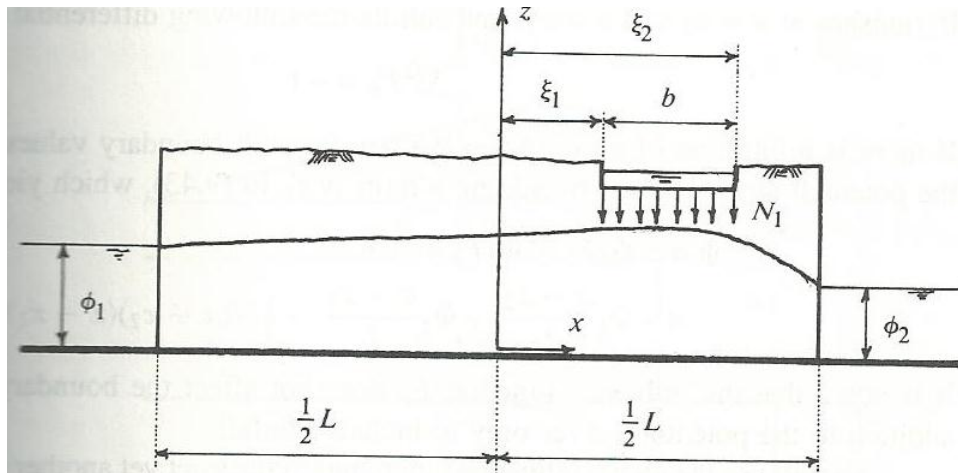


**Figure 1.3: Schematic on shallow unconfined flow with infiltration (Stark,1989).**

### 1.3 Numerical Models

Numerical models simulate hydrologic systems using numerical equations with defined boundary conditions (Fetter, 2001). They allow systems with complex boundary conditions and/or heterogeneity to be modeled, but they require more data, time, and money to produce than traditional analytical models (Fetter, 2001). Many numerical models have been developed for atmospheric, groundwater, and surface water hydrologic systems, which are currently used such as MODFLOW, FEFLOW, and ParFlow (DHI-WASY Software, 2012; Harbaugh, 2000; Maxwell, 2010).

### 1.3.1 ParFlow

ParFlow is a parallel, variably-saturated groundwater flow model that simulates subsurface flow by solving Richard's equation in three dimensions. It uses a multigrid-preconditioned conjugate solver (Ashby, 1996) and a Newton-Krylov nonlinear solver (Jones, 2001). ParFlow requires as inputs specification of subsurface hydraulic properties, such as the saturated hydraulic conductivity, porosity, and the van Genuchten parameters for the pressure-saturation relationships.

ParFlow simulates overland flow using the kinematic wave equation and is coupled with the Community Land Model to simulate fully coupled land surface processes. Thus ParFlow has the unique ability to explicitly resolve streamflow without the use of parameterized river routing subroutines. This allows rivers and streams in the domain to develop naturally based on topographic gradients. ParFlow's ability to model complex structures such as topography, hydrologic facies, heterogeneous porous media, and watershed boundaries for a three-dimensional domain make it well suited for modeling high-resolution, large-scale problems (Maxwell, 2010).

## 1.4 Hydraulic Residence and Response Time

Hydraulic residence and response times are of interest for many hydrologic systems, because they describe the unique reactions of a hydrologic system. A hydrologic system such as the Santa Fe Group Aquifer incorporates the interactions of groundwater water, alluvial sediments, recharge zone(s), discharge zone(s), and surface water (Alley, 2002). The time it takes water to travel from recharge zone(s) to discharge zone(s) in a groundwater system is referred to as the system's *hydraulic residence time*,  $\tau$  (Cohen, 2011). Hydraulic residence time can vary greatly between different study areas because it is based on aquifer and stream properties unique to each site, and is defined by:

$$\tau = \frac{V}{Q} \tag{2.19}$$

where  $V$  is the volume, and  $Q$  is the flow rate (Cohen, 2011).

The time required for piezometric heads in an aquifer to come to equilibrium with a hydraulic perturbation, such as changes in stream flow, is the *hydraulic response time*,  $T$ , and is defined by:

$$T^* = S_s L_c^2 / K \quad (2.20)$$

where  $T^*$  is the hydraulic response time (T),  $S_s$  is the specific storage ( $L^{-1}$ ),  $L_c$  is the distance between the point of interest and the stream (L), and  $K$  is the hydraulic conductivity ( $LT^{-1}$ ) (Alley, 2002).

## **CHAPTER 2: PURPOSE AND SCOPE**

The goal of this MS thesis research is to quantify parametric sensitivity between interactions in the Santa Fe Aquifer Group and the Rio Grande using a combination of observations and modeling. This is comprised of four objectives. The first objective is to document data collection methods. Second, a simple graphical analysis of the high frequency pressure and temperature data is performed to qualitatively investigate the response of the Santa Fe Aquifer Group and Rio Grande. Individual piezometers, piezometer nests, transects, and surface water stage, are compared in order to chose a cross section for further study. The third objective is to develop three hydrologic models of increasing complexity for the selected cross-section for comparison. The approaches used are: 1) an analytical model using Darcy's Law for steady-state conditions, 2) a two-dimensional homogenous subsurface ParFlow model, and 3) a two-dimensional layered subsurface ParFlow model. The Darcy flux is calculated using each approach.

## CHAPTER 3: STUDY AREA

This research focuses on the relationships between the Santa Fe Group Aquifer System and the Rio Grande. In order to study these relationships, a study area, covering approximately 20 miles, was chosen in the Albuquerque, NM metropolitan area, which is within the Middle Rio Grande Basin.

### 3.1 Geology

#### *3.1.1 Rio Grande Rift and Middle Rio Grande Basin*

The Rio Grande Rift is an area of Cenozoic crustal extension beginning in Mexico and extending into central Colorado (McAda, 2002). The rift formation began 25 million years ago and initially consisted of a succession of topographically closed basins (Bartilino, 2002) with uplifts occurring along the eastern and western edges of the rift. Over time, sediment from adjacent mountain ranges, wind-blown sands, and volcanic sediments deposited in the closed basins (Bartilino, 2002) producing in some areas, sedimentary basin fill as thick as 7.1 miles (Plummer, 2004).

The Middle Rio Grande Basin (MRGB), one in a series of basins created by the Rio Grande Rift (McAda, 2002), is located in central New Mexico. The basin covers about 3,060 square miles (Bexfield, 2001) stretching from the Jemez Mountains in the north to La Joya Hills and Ladron Peak in the South (Plummer, 2004); in the east, the basin is bounded by the Sandia, Manzano, and Los Pinos Mountains (Plummer, 2004), which are composed of Precambrian plutonic and metamorphic rocks, unconformably overlain by Paleozoic limestone, sandstone, and shale (McAda, 2002); and in the west the MRGB is bounded by the Lucero uplift, which is composed of Paleozoic limestone, sandstone, and shale and Cenozoic Basalt flows, and the Nacimiento uplifts, which is composed of Precambrian plutonic and metamorphic rocks (Plummer, 2004; McAda, 2002).

#### *3.1.2 Santa Fe Group and the Santa Fe Group Aquifer System*

The central MRGB consists primarily of unconsolidated to moderately consolidated basin-fill sediments, known as the Santa Fe Group (Plummer, 2004). These alluvial deposits are a complex mixture of sediment types and grain sizes that vary horizontally and vertically in

extent (Bartilino, 2002). Sediments of the Santa Fe Group can be separated into three layers: lower, middle, and upper.

#### 3.1.2.1 Lower Santa Fe Group

The lower Santa Fe Group sediments range in age from 30 to 15 million years old and are primarily composed of interlaced piedmont-slope, eolian, and fine-grained basin-floor deposits (Hawley, 1992). Fan and calescent-fan alluvium characterize the piedmont-slope deposits, whereas the basin floor deposits are described by playa sediments and playa margin. The Lower Santa Fe Group sediments represent deposition within an endorheic basin prior to deep subsidence and uplift caused by the Rio Grande Rift (Hawley, 1992).

#### 3.1.2.2 Middle Santa Fe Group

The middle Santa Fe Group was deposited during a period when tectonism was most active in the MRGB, around 15 and 5 million years ago. Piedmont-slope sediments continued to be deposited at the margins of the basin, but sediments were also transported into the MRGB by large fluvial systems flowing from the north, northeast, and south west. As a result of high tectonic activity and sedimentation rates, the bulk of the Santa Fe Group was deposited during this period (Hawley, 1992).

#### 3.1.2.3 Upper Santa Fe Group

After approximately 5 million years, the ancestral Rio Grande and two of its tributaries, the Rio San Jose and Rio Puerco, formed a large aggradational plain in the central basin area. Over the next four million years the upper Santa Fe Group sediments were deposited, consisting primarily of interlaced piedmont-slope and fluvial basin-floor, deposits. Piedmont-slope deposits (alluvial and debris-flow) were comprised of poorly sorted, weakly stratified sand and conglomerate. The basin-floor deposits contained cross-stratified ancestral river sediments, which can be characterized by concentrated areas of clean sand and pebble gravel. Fine- to medium-grained overbank sediments were deposited in confluences of the large river system and in basin-floor and piedmont-slope transition zones (Hawley, 1992).

#### 3.1.2.4 Santa Fe Group Aquifer System

The Santa Fe Group, in addition to younger alluvial deposits along the Rio Grande form the Santa Fe Group Aquifer system (Bartilino, 2002). The Santa Fe Group Aquifer System is the largest aquifer within the MRGB (Bexfield) and is as much as 14,000 ft thick in the Albuquerque, NM area (McAda, 1996). The aquifer system is composed primarily of middle Tertiary to Quaternary Santa Fe Group and Quaternary post-Santa Fe Group sediments (McAda, 1996). The Upper, Middle, and Lower Santa Fe Group sediments are approximately 1,500, 9,000, and 3,500 ft thick, respectively (McAda, 1996).

The Santa Fe Group Aquifer system is hydraulically connected to the Rio Grande through the inner valley alluvium (McAda, 1996). The most permeable aquifer zones are within the upper part of the Santa Fe Group, which is composed of channel sediments deposited by the ancestral Rio Grande. These deposits are largely composed of sand and gravel that result in relatively large hydraulic-conductivity values, ranging from 30 to greater than 100 feet per day (McAda, 1996).

### **3.2 Rio Grande**

The present-day, Rio Grande is the fifth largest river in North America (Bartilino, 2002) extending from the San Juan Mountains in southwestern Colorado (Plummer, 2004) to the Gulf of Mexico. It serves as the primary surface water drainage for the MRGB. Similar to many other modern day rivers, flow in the Rio Grande is controlled by a series of dams, reservoirs, and an intricate network of irrigation canals, ditches and drains, which have been developed over the last 90 years (Bartilino, 2002). The riverside drains were installed during the 1920's and 1930's as a method to intercept seepage from the Rio Grande, which in turn would prevent flooding and water logging of the irrigated fields (McAda, 1996).

The Rio Grande system is regulated by an interstate compact between Colorado, New Mexico and Texas, called the Rio Grande Compact, which was adopted in 1939. This document defines the amount of water that is to be delivered to New Mexico and Texas and sets a minimum quality requirement.

### **3.3 Climate**

The Middle Rio Grande Basin varies in elevation from the valley floor to 11,000 feet along its northern, eastern and southern edges (Bexfield, 2001). This vast change in elevation causes a complex graduation of climate and ecological communities within the basin. The climate for much of the central MRGB is classified as desert (Bartilino, 2002) to semiarid while neighboring mountain regions are classified as humid continental (Plummer, 2004).

Evapotranspiration within in the basin is generally large relative to precipitation and most recharge within in the basin occurs as mountain-front recharge and infiltration from the Rio Grande system (Bexfield, 2001). Annual precipitation and snowfall were measured in two locations within the Albuquerque Basin from 1914 to 2003: (1) Albuquerque, NM at an elevation of 1,168m and (2) Sandia Park at an elevation of 2,139 m. Mean annual precipitation for Albuquerque, NM and Sandia Park was 55.3 inches and 122.7 inches, respectively. Mean annual snowfall for Albuquerque, NM and Sandia Park was 63.8 inches and 378.5 inches, respectfully (Plummer, 2004).

Eight main plant communities are listed for the present-day MRGB and surrounding mountains. In progression from the valley to mountain summit, the plant communities are riparian woodland, desert grasslands, plain-mesa grasslands, scrublands, juniper savanna, piñon-juniper woodlands, ponderosa pine, subalpine, and mixed coniferous forest (Bartilino, 2002). The vegetation of the riparian woodland (or bosque) has evolved significantly since the introduction of exotic species prior to 1900 and the construction of flood-control and bank stabilization projects.

### **3.4 Description of Study Area**

The study area falls within the Albuquerque Basin (Figure 3.1). Site locations are along the Rio Grande throughout the Albuquerque, NM metropolitan area from the Alameda bridge in the northern portion of the city to the Interstate 25 bridge at its southern edge. The eastern and western bounds of the study area are within the inner valley adjacent to the Upper Corrales, Corrales, Albuquerque and Atrisco Riverside drains. The inner valley is approximately 2-3 miles wide and includes the Rio Grande riparian zone, a densely vegetated region of land bordering the Rio Grande. The inner valley slopes 5-6 feet per mile southward through the Albuquerque area.

The riverside drains parallel to the Rio Grande are generally separated from the river by levees and are designed to intercept lateral groundwater flow from the river (Rankin, 2011).

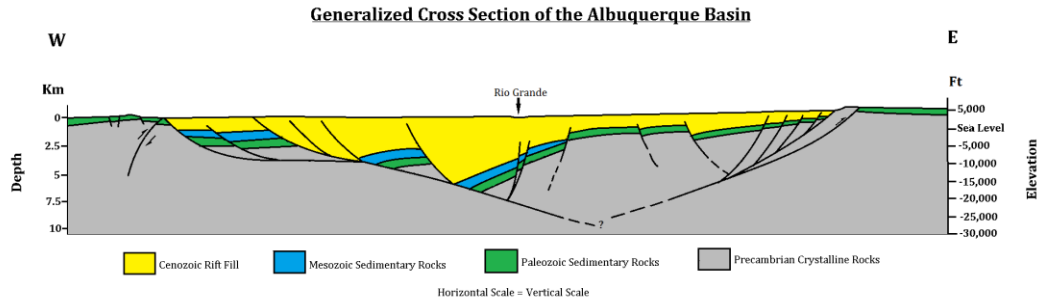


**Figure 3.1: Generalized cross-section of the Albuquerque Basin (Russel, 2002).**

### 3.5 Middle Rio Grande Valley Monitoring Network

The Middle Rio Grande Valley Monitoring Network (MRGVM) was established in 2003, through the collaboration of the United States Geologic Survey (USGS), Middle Rio Grande Endangered Species Collaborative Program, and United States Army Corps of Engineers (Rankin, 2011). Eight cross-sections were created over a five-year period at select locations along the Rio Grande. Figure 3.1 shows the cross-section locations from north to south: Alameda, Paseo Del Norte, Montano, Barelvas, Central, Rio Bravo, Pajarito, and Interstate 25. Cross-sections are composed of two transects of piezometer nests (multiple monitoring wells with screen openings at different depths) oriented perpendicular to the Rio Grande. A plan view of the Barelvas cross-section is shown in Figure 3.2 and described in Table 3.1. The northern and southern transects are separated by approximately 500 feet and spanned from west of the west riverside drain to east of the east riverside drain. Each transect is constructed of between six and ten piezometer nest depending on the spatial location.

Each piezometer nest includes between one and three piezometers (monitoring well screened for a five-foot interval completely below the water table) depending on the location. Shallow piezometers (indicated by “s” in Figure 3.2) were drilled to a completion depth of 15 to 25 ft and screened for five feet at a depth between 5-15ft Mid piezometers (indicated “m” in Figure 3.2) were drilled to a completion depth of 25 to 35 ft and screened over five feet between 20-30 ft Deep piezometers (indicated “d” in Figure 3.2) were drilled to a completion depth of 40 to 55 ft and screened for five feet between 35-50 ft Surface water gages were installed in the Rio Grande east riverside and west riverside drains.

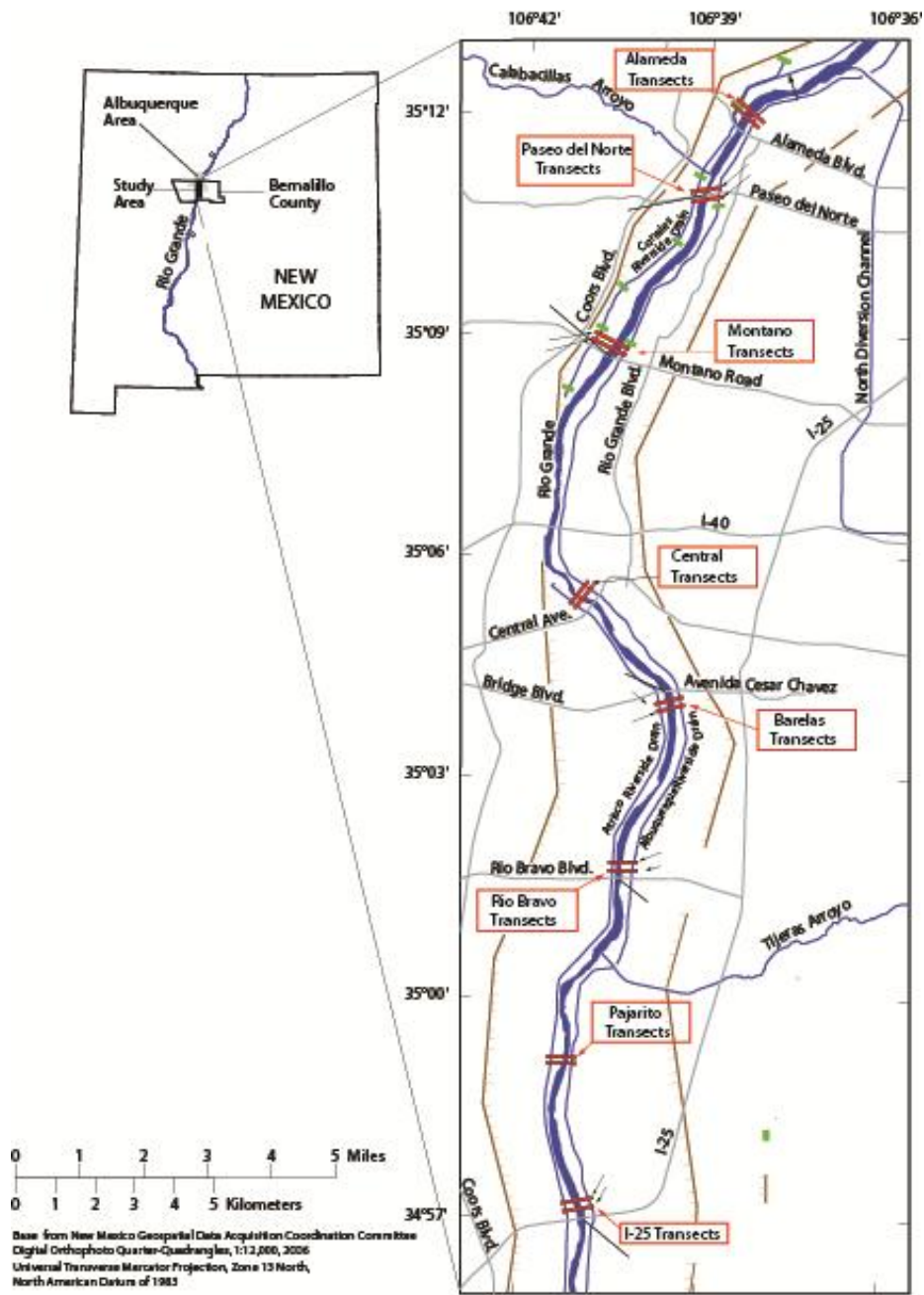
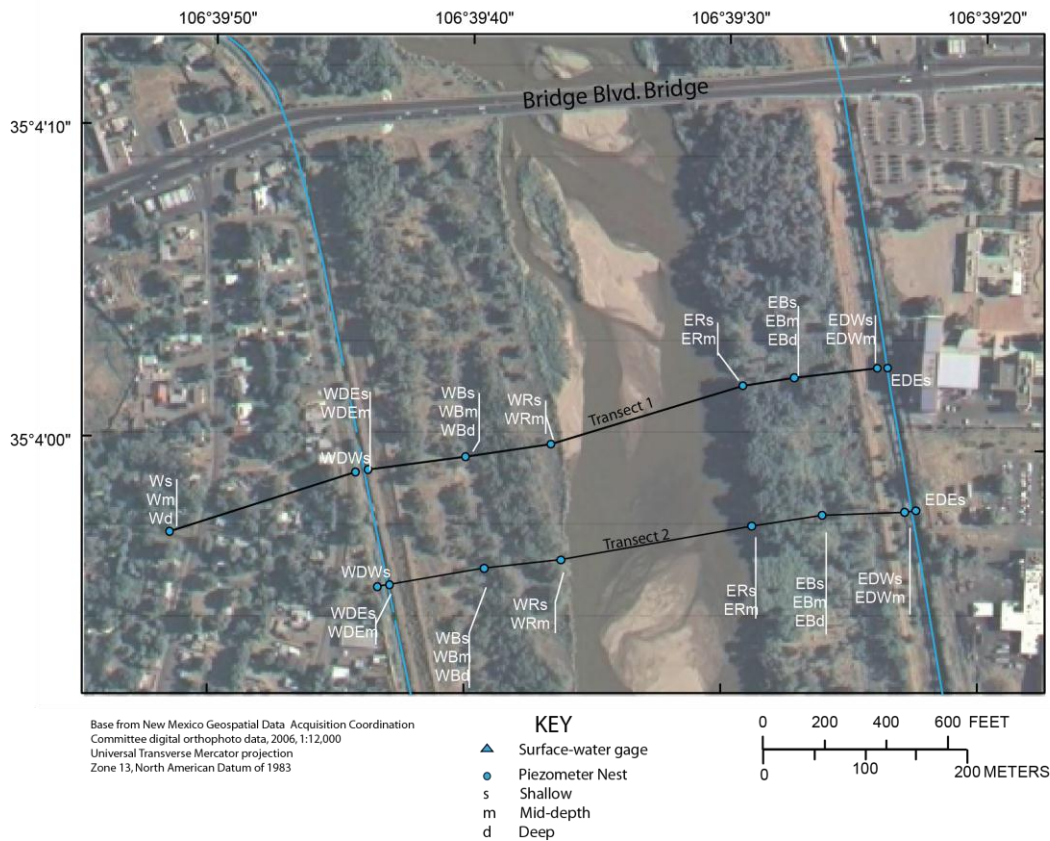


Figure 3.2: Middle Rio Grande Valley Monitoring Network (Rankin, 2011).



**Figure 3.3: Plan view of the Barelas cross-section (adapted from Rankin, 2011).**

**Table 3.1: Description of piezometer nest names and locations**

Site Name	Site Name Abbreviation	Description of Location
West	W	West of the western riverside drain
West Drain Westside	WDW	Adjacent to the west riverside drain on the western side
West Drain Eastside	WDE	Adjacent to the west riverside drain on the eastern side
West Bosque	WB	In the bosque west of the Rio Grande, between the river and the west riverside drain
West River	WR	Adjacent to the Rio Grande, west of the river
East River	ER	Adjacent to the Rio Grande, east of the river
East Bosque	EB	In the bosque east of the Rio Grande, between the river and the east riverside drain
East Drain Westside	EDW	Adjacent to the east riverside drain on the western side
East Drain Eastside	EDE	Adjacent to the east riverside drain on the eastern side
East	E	East of eastern riverside drain

### **3.6 Barelás Cross-Section**

The Barelás cross-section was established adjacent to the Bridge Blvd Bridge in central Albuquerque, NM during late 2005 and early 2006. It is located at 35°04'01.9 north, 106°39'29.3 west, and an elevation of 4942 ft above sea level (asl). It is composed of seventeen piezometer nests and three surface water gages (see Figure 3.2).

The Barelás cross-section was chosen for this study because of its location, duration of record, and types of available data. It is centrally located within the study area, reflecting a mixture of 1) the coarse grain and cobble materials observed in the study area's northern reach and 2) the fine grain materials and more prevalent clay stringers observed in the southern reach of the study area. This is a well-established cross-sections with data available for most piezometer nests from spring 2006 to present. All of the collected data types, geologic coring data, high frequency pressure and temperature data, and slug test data, are available at the Barelás cross-section. This is unlike more recently established cross-sections, such as Alameda or Central, and furthermore supports the selection of this specific cross-section.

## CHAPTER 4: METHODS

### 4.1 Data Collection

The USGS collected several types of data to perform a detailed characterization of the hydrogeology of the riparian area adjacent to the Rio Grande through its Albuquerque, NM reach. Firstly, coring data was collected during the drilling process for select piezometer locations. Secondly, each piezometer was instrumented with an In-Situ Level Troll to collect high frequency pressure and temperature data: In-Situ Minitroll, In-Situ T300, and In-Situ T500. Thirdly, slug tests were performed at select piezometer locations.

#### *4.1.1 Geologic Coring Data*

Piezometers were installed using direct-push drilling technology. Continuous subsurface core samples were collected during piezometer installation from a subset of the piezometer locations from the Paseo Del Norte, Montano, Barelás, Rio Bravo, and Interstate 25 transects. Core samples were generally collected from the deepest piezometer in the river, Bosque, and inner riverside drain piezometer nests. Each core sample was collected in an acetate tube for preservation and described in the field.

#### *4.1.2 High Frequency Pressure and Temperature Data*

Piezometer and surface water gages were instrumented with vented and unvented submersible pressure transducers (In-Situ Minitroll, T300, or T500) to collect continuous hourly pressure data. Each probe is completely sealed and includes a pressure sensor, real-time clock, microprocessor, lithium battery, data logger, memory, a vented or unvented RuggedCable System, and desiccant. The vented In-Situ T500 transducers automatically compensate for barometric pressure changes. The unvented Minitroll and T300 transducers require a post-processing barometric pressure correction. The In-Situ T500, T300, and some of the Minitroll probes are capable of measuring water temperature in addition to pressure. Hourly water temperature was also collected at locations where the submersible pressure transducer was capable of measuring temperature.

#### 4.1.3 Slug Test Data

Slug tests were performed at selected piezometer locations throughout the study area. A 60-inch long, 0.75-inch diameter, weighed polyvinyl chloride (PVC) slug was rapidly introduced to the 1-inch diameter piezometers to produce a positive displacement of water. Water levels in the piezometers were recorded at one-second intervals before, during, and after the introduction of the slug. Hydraulic conductivity estimates were determined by the Bouwer and Rice (1976) and the Bulter (1998) methods for slug-test analysis in unconfined aquifers.

#### 4.2 ParFlow Models

In order to further investigate groundwater-surface water interactions within the study area, the Barelás Cross-section was modeled using ParFlow assuming three model subsurface configurations: homogenous, layered, and a correlated, Gaussian random field. The domain was consistent for the three scenarios and was modeled as a two-dimensional cross-section of the Barelás Transect 1 piezometer locations. The model domain is 12,600 ft across and centered on the Rio Grande (see Figure 4.1). The simulated domain extends from the land surface to the upper interface of the Santa Fe Aquifer Group, traversing a total 120 vertical feet. The system was modeled using a horizontal grid resolution of 10 feet and a vertical resolution of 1 foot.

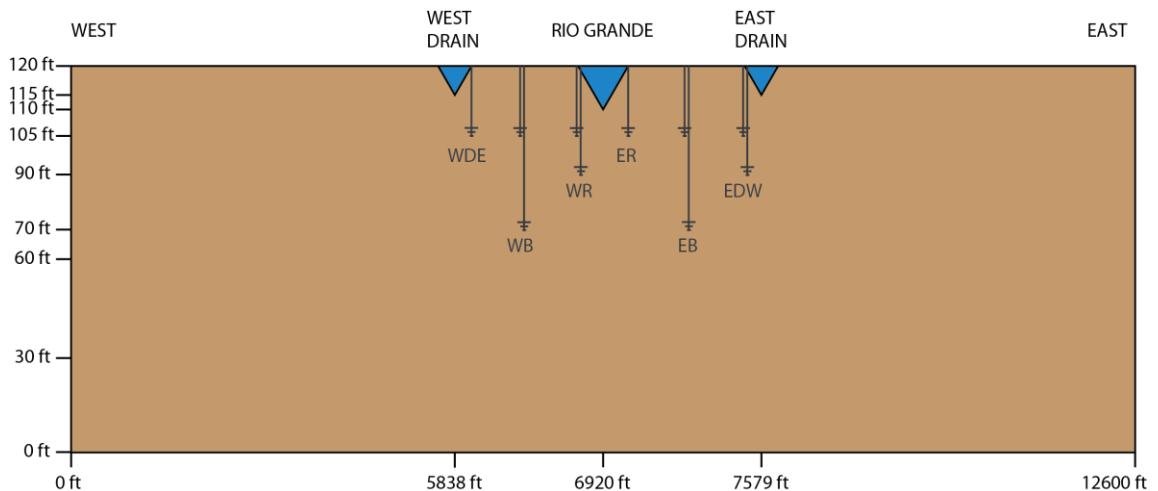


**Figure 4.1: Cross-section schematic of ParFlow model domain (not to scale).**

Ten inner Bareltras transect 1 piezometers (monitoring wells between east and west riverside drains) were incorporated into the model for comparison with the observed high frequency pressure data. The piezometers varied in distance from the river and the depth of their screened interval as is described in Table 4.1. The distance between the piezometers and the river ranged from 17-913 ft. The measurement point depth for the shallow, mid, and deep piezometers ranged in depth below land surface (bls) from 5-7 ft, 20-22 ft, and 42 ft, respectively.

**Table 4.1: Description of piezometers include in ParFlow models.**

Well Name	Well Identifier	Model X Node Location	Model Z Node Location	Actual Distance from the River to Piezometer (ft)	Measuring Point Depth (ft bls)
West Drain Eastside Shallow	WDEs	585	114	913	6
West Bosque Shallow	WBs	623	113	534	7
West River Shallow	WRs	648	113	289	7
East River Shallow	ERs	709	115	17	5
East Bosque Shallow	EBs	729	114	218	6
East Drain Westside Shallow	EDWs	754	115	467	5
West River Mid	WRm	648	98	289	22
East Drain Westside Mid	EDWm	754	100	467	20
West Bosque Deep	WBd	623	78	534	42
East Bosque Deep	EBd	729	78	218	42

The western, eastern, upper and lower domain patches were simulated as a constant flux boundaries, where the flux was 0 feet per hour (ft/hr), making them no flow boundaries. The model assumed that evaporation or transpiration are not present in the system and that all the water entering the system is through the river patches.

Each model is simulated for two years using the Rio Grande stage as the model forcing. The 2006-2007 water year (Oct. 1, 2006 to Sept. 30, 2007) is used for the simulation and repeated twice: first for one year of spin up and then one year of model run. Time was incremented hourly, resulting in 8,760 time steps. The initial pressure for the spin up run was assumed to be 10 ft below land surface (bls). The last pressure file of the spin up run is used as the initial pressure condition for the model run.

#### 4.2.1 Homogenous Model Simulations

The homogenous subsurface models are created in ParFlow assuming a bulk hydraulic conductivity and bulk specific storage for the entire domain (see Figure 4.2). Twenty-one scenarios were modeled in total and the parameter values for each scenario are described in Table 4.2. The bulk hydraulic conductivity values ranged from 0.083 ft/hr (2 ft/day) to 20 ft/hr (480 ft/day) and were chosen based on slug test data collected for the study area. Although a range of bulk hydraulic conductivity values were determined from the slug test results, very little is known about the range of specific storage values at the Barelas Transect 1 piezometer locations. Therefore, three values of specific storage were tested spanning three orders of magnitude from  $3.048 \times 10^{-5}$  to  $3.048 \times 10^{-7} \text{ ft}^{-1}$ .

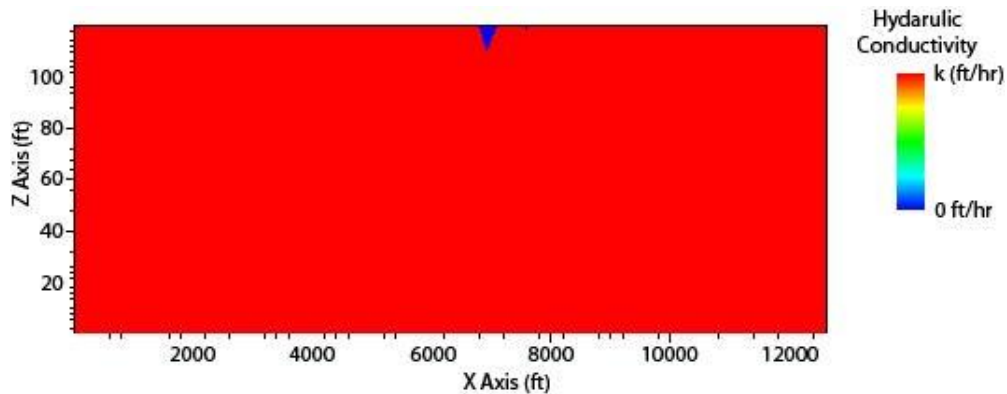


**Figure 4.2: Homogenous subsurface model domain, (note: 225 times vertical exaggeration).**

#### 4.2.2 Layered Subsurface Models

The layered subsurface models were created in ParFlow assuming a bulk hydraulic conductivity for each sediment type and a bulk specific storage value for the entire domain. The parameter values used for each scenario are described in Table 4.3. Figure 4.3 shows the thickness and number of layers modeled. Layers are based on geologic coring data from the Barelas cross-section collected during piezometer installation.

**Table 4.2: Description of parameters used homogenous subsurface model scenarios.**

Model Number	Bulk Hydraulic Conductivity (ft/hr)	Specific Storage ( $ft^{-1}$ )
1	0.083	$3 \times 10^{-5}$
2	0.083	$3 \times 10^{-6}$
3	0.083	$3 \times 10^{-7}$
4	0.417	$3 \times 10^{-5}$
5	0.417	$3 \times 10^{-6}$
6	0.417	$3 \times 10^{-7}$
7	2.042	$3 \times 10^{-5}$
8	2.042	$3 \times 10^{-6}$
9	2.042	$3 \times 10^{-7}$
10	3.750	$3 \times 10^{-5}$
11	3.750	$3 \times 10^{-6}$
12	3.750	$3 \times 10^{-7}$
13	10.000	$3 \times 10^{-5}$
14	10.000	$3 \times 10^{-6}$
15	10.000	$3 \times 10^{-7}$
16	15.000	$3 \times 10^{-5}$
17	15.000	$3 \times 10^{-6}$
18	15.000	$3 \times 10^{-7}$
19	20.000	$3 \times 10^{-5}$
20	20.000	$3 \times 10^{-6}$
21	20.000	$3 \times 10^{-7}$

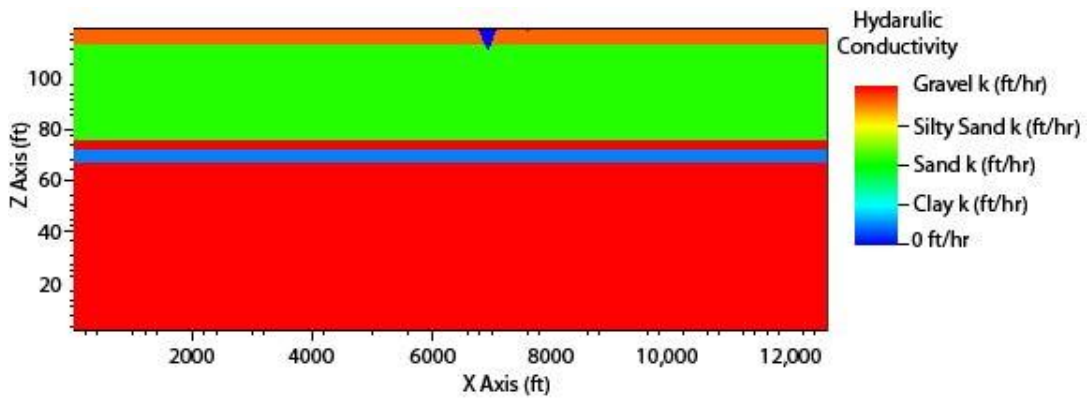


**Figure 4.3: Layered subsurface model domain, (note: 225 times vertical exaggeration).**

**Table 4.3: Description of parameters used for layered subsurface models.**

Model Scenario Number	Sediment Name	Soil Type Hydraulic Conductivity (ft/hr)	Geometric Mean Hydraulic Conductivity (ft/hr)	Specific Storage (ft <sup>-1</sup> )
22	Silty Sand	10.780	15.0	3x10 <sup>-5</sup>
	Sand	18.000		
	Clay	2.500		
	Gravel	20.000		
23	Silty Sand	10.780	15.0	3x10 <sup>-6</sup>
	Sand	18.000		
	Clay	2.500		
	Gravel	20.000		
24	Silty Sand	10.780	15.0	3x10 <sup>-7</sup>
	Sand	18.000		
	Clay	2.500		
	Gravel	20.000		
25	Silty Sand	4.540	15.0	3x10 <sup>-5</sup>
	Sand	20.000		
	Clay	0.083		
	Gravel	40.000		
26	Silty Sand	4.540	15.0	3x10 <sup>-6</sup>
	Sand	20.000		
	Clay	0.083		
	Gravel	40.000		
27	Silty Sand	4.540	15.0	3x10 <sup>-7</sup>
	Sand	20.000		
	Clay	0.083		
	Gravel	40.000		
28	Silty Sand	3.750	15.0	3x10 <sup>-5</sup>
	Sand	17.500		
	Clay	0.417		
	Gravel	40.000		
29	Silty Sand	3.750	15.0	3x10 <sup>-6</sup>
	Sand	17.500		
	Clay	0.417		
	Gravel	40.000		

**Table 4.3 Continued**

Model Scenario Number	Sediment Name	Soil Type Hydraulic Conductivity (ft/hr)	Geometric Mean Hydraulic Conductivity (ft/hr)	Specific Storage (ft <sup>-1</sup> )
30	Silty Sand	3.750	15.0	3x10 <sup>-7</sup>
	Sand	17.500		
	Clay	0.417		
	Gravel	40.000		
31	Silty Sand	2.042	15.0	3x10 <sup>-5</sup>
	Sand	20.000		
	Clay	0.083		
	Gravel	61.350		
32	Silty Sand	2.042	15.0	3x10 <sup>-6</sup>
	Sand	20.000		
	Clay	0.083		
	Gravel	61.350		
33	Silty Sand	2.042	15.0	3x10 <sup>-7</sup>
	Sand	20.000		
	Clay	0.083		
	Gravel	61.350		

*4.2.3 Random Field Models*

The random field subsurface models are created in ParFlow using a correlated, Gaussian random field approach via the Turning Bands method (Tompson et al., 1989), where a permeability value is assigned to each node within the domain. A geometric mean of hydraulic conductivity of 15 ft/hr is used and bulk specific storage value for the entire domain. The parameter values used for each scenario are described in Table 4.4.

**Table 4.4: Description of parameters used in random field subsurface model scenarios.**

Model Number	Geometric Mean Hydraulic Conductivity (ft/hr)	Vertical Correlation (ft)	Horizontal Correlation (ft)	Variance lnK	Specific Storage (ft <sup>-1</sup> )
34	15.0	5.0	50.0	1.0	$3 \times 10^{-5}$
35	15.0	5.0	50.0	1.0	$3 \times 10^{-6}$
36	15.0	5.0	50.0	1.0	$3 \times 10^{-7}$

## **CHAPTER 5: GRAPHICAL ANALYSIS OF THE OBSERVED VALUES FOR THE BARELAS CROSS-SECTION**

High frequency pressure data was collected by the USGS from approximately 250 piezometers throughout the Albuquerque, NM area. Figure 5.1 presents water table elevation for the duration of record at the Barelas Transect 1 piezometer locations. The data has been plotted on nine separate subplots in order to compare trends at different piezometer nest locations. The uppermost subplot shows the data collected from the three surface water gages at the Barelas cross-section, where the Rio Grande, east riverside drain, and west riverside drain are represented by a black solid line, red dashed-dotted line, and a blue dotted line, respectively. The remaining eight subplots show the piezometer data at the eight piezometer nest locations from east to west, where the shallow, mid, and deep piezometers are represented by a black solid line, red dashed-dotted line, and a blue dotted line, respectively.

It should be noted that the range of values observed for the surface water gages and the piezometer nests vary less than 10 ft for the duration of record. The Rio Grande surface water gage displays a strong seasonal signal. The peak surface water stage each year corresponds to spring runoff in NM. The late summer months display a higher frequency of smaller peaks, likely related to storm events during the summer monsoons.

A spatial relationship between the piezometer signal and the piezometer's distance from the river can be observed. The piezometer nests closer to the river (ER and WR) have a more similar signal to the Rio Grande signal than piezometer nest further from the river. As the distance between the piezometer nest and the river increases dampening and lag in the piezometer signal increases. This is easily observed for the East River (17 ft from river), East Bosque (218 ft from river), and East Drain Westside (467 ft from river) piezometer plots. In May 2008, there is a large peak in the river discharge. The East River site closely mimics the river signal for this period. There appears to be almost no lag and the high frequency, short duration peaks are preserved in the East River piezometer signal. In contrast, the East Drain Westside piezometer is a smoother (dampened) signal and appears to have a lag of several days from the river signal.

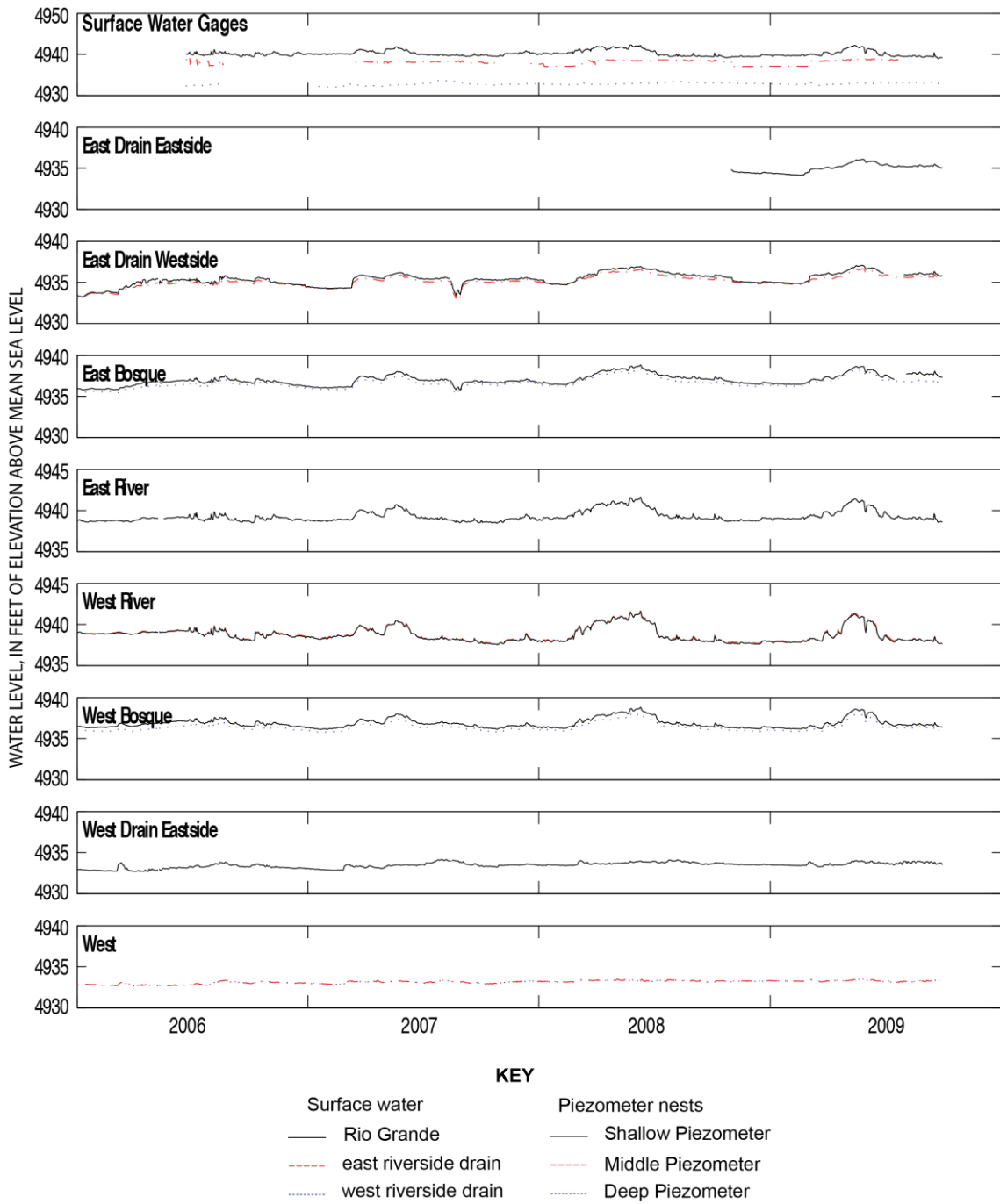


**Figure 5.1: Water table elevation at the Barelas Transect 1 Piezometers for a four-year duration.**

The average and standard deviation were calculated for each piezometer location and the Rio Grande for the 2006-2007 water year. Table 5.1 shows the observed average and standard deviation values. The Rio Grande has an average elevation of 4,940.21 feet above sea level (ft asl) and standard deviation of 0.52 for the 2006-2007 water year. The average water table elevation ranges approximately 6 ft for the Barelás Transect 1 Piezometers. The lowest, average water table elevation was observed at the piezometer furthest from the Rio Grande, WDEs. Figure 5.2 shows a comparison of standard deviation with piezometer distance from the river. Standard deviation values ranged from 0.33 to 0.62 for the Barelás 1 transect piezometer. The lowest variation from the average was observed at the WDEs piezometer nest. This finding is intuitive because, as previously stated, the WDEs piezometer showed the most damping from the original river signal.

**Table 5.1: Average and standard deviation for the observed values (ft asl).**

Site Name	Piezometer ID	Average (ft asl)	Standard Deviation (ft)
Rio Grande	RGsw	4940.21	0.52
West Drain East Shallow	WDEs	4933.38	0.33
West Bosque Shallow	WBs	4936.81	0.43
West River Shallow	WRs	4938.71	0.61
East River Shallow	ERs	4939.16	0.51
East Bosque Shallow	EBs	4936.78	0.53
East Drain Westside Shallow	EDWs	4935.14	0.61
West River Mid	WRm	4938.77	0.62
East Drain Westside Shallow	EDWm	4934.91	0.53
West Bosque Deep	WBd	4936.35	0.37
East Bosque Deep	EBd	4936.43	0.47

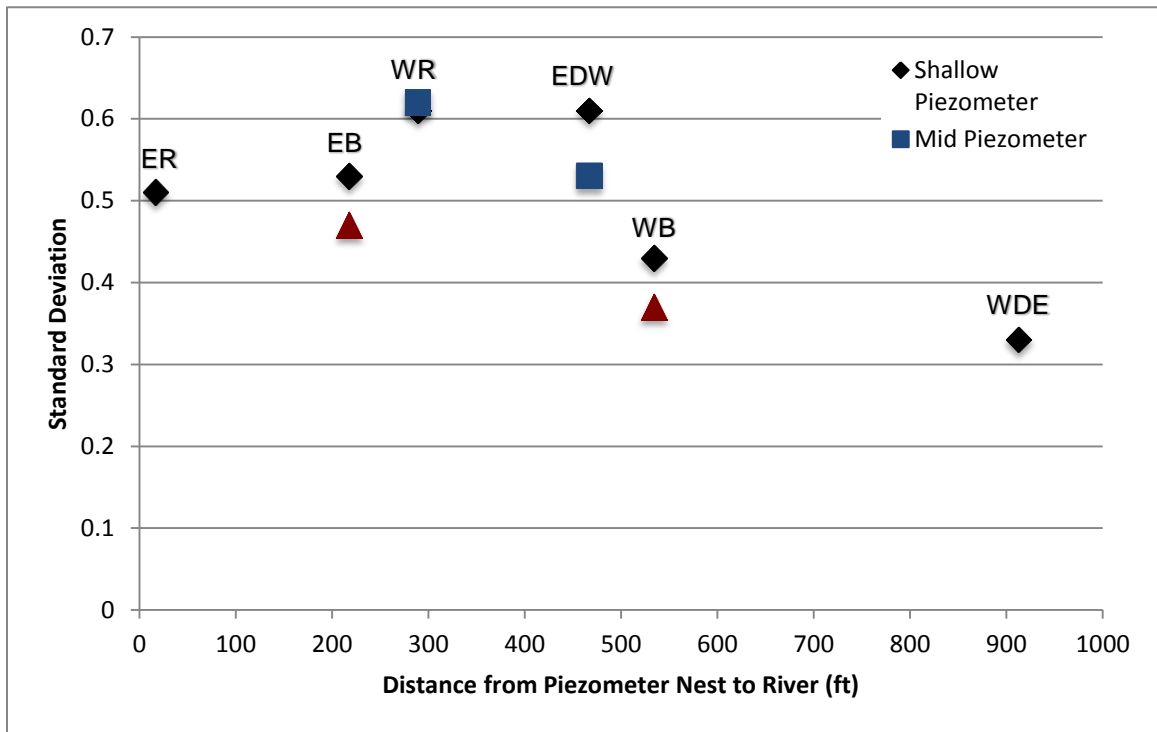


Figure 5.2: Comparison of standard deviation and distance from piezometer to the river.

**CHAPTER 6: DISCUSSION OF RIVER LEAKAGE FOR MIDDLE RIO GRANDE  
VALLEY MONITORING NETWORK**

The rate of river leakage from the Rio Grande is calculated for each of the Middle Rio Grande Valley Monitoring Network cross-sections using an average hydraulic conductivity and horizontal hydraulic gradient value. Hydraulic conductivity estimates for the study area are determined using the Bouwer and Rice (1976) and the Bulter (1998) slug-test analysis methods for unconfined aquifers (Rankin, 2011). Estimated values range from 2 ft/day at the Pajarito cross-section to 240 ft/day at the Central cross-section. The hydraulic conductivity values were grouped into three categories, and then averaged: piezometers east of the Rio Grande, piezometers west of the Rio Grande, and all the piezometers within a cross-section. The average hydraulic conductivities are shown in Table 6.1. The average cross-section hydraulic conductivity ranges from 39 ft/day at the Barelmas and Pajarito cross-sections to 140 ft/day at the Central cross-section.

**Table 6.1: Mean hydraulic conductivities estimated from slug tests, feet per day.**

<b>Cross-section Name</b>	<b>Eastside</b>	<b>Westside</b>	<b>Cross-section</b>
Alameda	55	35	45
Paseo del Norte	40	60	50
Montano	65	10	41
Central	170	110	140
Barelmas	27	65	49
Rio Bravo	47	33	39
Pajarito	46	31	39
Interstate 25	63	70	65

The daily horizontal hydraulic gradients and groundwater flow direction are calculated using an adaptation on the three-point method and the daily-mean groundwater levels from the inner Transect one and Transect two piezometers (Rankin, 2011). The daily hydraulic gradients are averaged for the period of collection and are presented in Table 6.2. Values range from  $2.54 \times 10^{-3}$  at the Interstate 25 Eastside to  $1.53 \times 10^{-2}$  at the Alameda Eastside. The averaged horizontal hydraulic gradient values vary from cross-section to cross-section, but also vary as much as an

order of magnitude within a cross-section. The Barelas cross-section has relatively constant hydraulic gradients for the entire cross-section.

**Table 6.2: Average horizontal hydraulic gradients (-).**

<b>Cross-section Name</b>	<b>Eastside</b>	<b>Westside</b>
Alameda	$1.53 \times 10^{-2}$	$4.47 \times 10^{-3}$
Paseo del Norte	$1.11 \times 10^{-2}$	$5.47 \times 10^{-3}$
Montano	$9.82 \times 10^{-3}$	$3.51 \times 10^{-3}$
Central	$6.58 \times 10^{-3}$	$4.39 \times 10^{-3}$
Barelas	$9.02 \times 10^{-3}$	$9.42 \times 10^{-3}$
Rio Bravo	$4.60 \times 10^{-3}$	$6.94 \times 10^{-3}$
Pajarito	$1.49 \times 10^{-2}$	$6.99 \times 10^{-3}$
Interstate 25	$2.54 \times 10^{-3}$	$5.25 \times 10^{-3}$

The average Darcy flux ( $q$ ) is calculated for each cross-section using equation 1.2 and the values are presented in Table 6.3. The Darcy flux values range from 0.04 feet per day (ft/day) at the Montano Westside to 1.12 ft/day at the Central Eastside. Values vary from cross-section to cross-section, but also within the cross-section between eastside and westside of the river.

**Table 6.3: Darcy flux calculations, feet per day.**

<b>Cross-section Name</b>	<b>Eastside</b>	<b>Westside</b>
Alameda	0.84	0.16
Paseo del Norte	0.44	0.33
Montano	0.64	0.04
Central	1.12	0.48
Barelas	0.24	0.61
Rio Bravo	0.21	0.23
Pajarito	0.68	0.22
Interstate 25	0.16	0.37

## CHAPTER 7: ANALYTICAL MODEL RESULTS

Three transient analytical models are used to calculate the water table elevation at five inner piezometer locations (WDE, WB, WR, ER, and EB): horizontal confined flow (eq. 1.4), horizontal unconfined flow (eq. 1.5), and shallow unconfined flow with infiltration (eq. 1.10). The average and standard deviation are calculated for the five piezometer locations for each of the transient analytical models and are shown in Table 7.1 and 7.2.

The average piezometer values range from 4932.82 ft asl to 4937.49 ft asl, 4922.63 ft asl to 4937.49 ft asl, and 4934.77 ft asl to 4935.98 ft asl for the horizontal confined flow analytical model, horizontal unconfined flow analytical model, and shallow unconfined flow with local infiltration analytical model, respectively. The lowest average values for all three analytical models were observed at the WDE piezometer nest (furthest piezometer nest). The analytic model averages varied from the observed values, but the difference does not appear to be directly related to the distance of the piezometer from the river or the depth of the piezometer. The shallow unconfined flow with local infiltration analytical model showed the smallest range in average values between piezometer locations.

**Table 7.1: Transient Analytical Model Averages**

Site	Observed	Horizontal Confined Flow	Horizontal Unconfined Flow	Shallow Unconfined Flow with Local Infiltration
WDE	4933.38	4932.82	4922.63	4934.77
WB	4936.81	4934.40	4928.45	4935.09
WR	4938.71	4935.43	4935.43	4935.29
ER	4939.16	4937.49	4937.49	4935.81
EB	4936.78	4935.31	4935.31	4935.98

The standard deviation values range from 0.13 to 0.60, 0.22 to 0.70, and 0.52 to 0.83 for the horizontal confined flow model, horizontal unconfined flow model, and shallow unconfined flow with local infiltration model, respectively.

**Table 7.2: Transient Analytical Model Standard Deviation**

Site	Observed	Horizontal Confined Flow	Horizontal Unconfined Flow	Shallow Unconfined Flow with Local Infiltration
WDE	0.33	0.13	0.70	0.52
WB	0.43	0.17	0.32	0.59
WR	0.61	0.22	0.22	0.65
ER	0.51	0.50	0.50	0.78
EB	0.53	0.60	0.60	0.83

The root mean squared error (RMSE) and mean absolute error (MAE) estimate the average error between observed and predicted values, but neither measure provides information about the relative size of the average difference or the type of differences. Unlike the RMSE and MAE, the index of agreement (d), is a descriptive measure that is relative and bounded (Willmont, 1982). Higher values of index of agreement represent better model fit. The index of agreement was calculated for all of the analytic model scenarios and the results are presented in Table 7.3.

The index of agreement values range from 0.22 to 0.53, 0.05 to 0.53, and 0.21 to 0.80 for the horizontal confined flow model, horizontal unconfined flow model, and shallow unconfined flow with local infiltration model, respectively. The best model fit was observed at the East Bosque Deep piezometer (EBd) location for all three models, whereas the worst model fit varied by location for the three analytical models.

**Table 7.3: Transient Analytic Models Index of Agreement**

Site	Horizontal Confined Flow	Horizontal Unconfined Flow	Shallow Unconfined Flow with Local Infiltration
WDES	0.49	0.05	0.26
WBS	0.22	0.07	0.32
WRS	0.23	0.23	0.22
ERS	0.37	0.37	0.21
EBS	0.47	0.47	0.69
WBD	0.24	0.07	0.37
EBD	0.53	0.53	0.80

## CHAPTER 8: NUMERICAL MODEL RESULTS

### 8.1 Average and Standard Deviation

The average and standard deviation of the predicted water level are calculated for all of the piezometer locations for the homogenous subsurface, layered subsurface, and random field subsurface ParFlow simulations.

The calculated average and standard deviation values for the homogenous subsurface models are shown in Tables 8.1-8.3. Bold values indicate the piezometer is closer to the Rio Grande and italicized values indicate the piezometer is further away from the Rio Grande. The average shallow piezometer values range from 4933.15 ft asl to 4939.19 ft asl. The lowest values were observed at the WDEs piezometer (furthest piezometer) and the highest values at the ERs piezometer (closest piezometer). The selected shallow piezometer standard deviation values range from 0.001 to 0.494 ft.

Lower bulk hydraulic conductivity values generally lead to smaller average and standard deviation values, underestimating the observed average and standard deviation. In contrast, higher bulk hydraulic conductivity values generally lead to larger average and standard deviation values, overestimating the observed average and standard deviation for each location. The bulk hydraulic conductivity values of 2.042 and 3.750 ft/hr do not follow this trend, which may be related to a lag in aquifer response to changes in the river due to the low saturated hydraulic conductivity and significant dampening of the pressure signal in these model runs.

When the bulk hydraulic conductivity is held constant and the specific storage is varied, generally there are relatively small differences in the calculated average and standard deviation values between scenarios. Changes in specific storage, appear to be more influential at larger bulk hydraulic conductivity values. These results indicate that the bulk hydraulic conductivity value is more influential on the calculated average and standard deviation than changes of specific storage for the range of values tested.

Additionally, a spatial comparison can be made between the three locations. The ERs piezometer, which is closest to the Rio Grande, has the least variation in average values between the different model scenarios, while the WDEs piezometer has the greatest variation. The range of standard deviation values remains relatively constant with varying distance from the river.

**Table 8.1: Average and standard deviation values for the homogenous subsurface models, the shallow piezometer locations are shown in the table.**

Model Number	Bulk Hydraulic Conductivity (ft/hr)	Specific Storage (ft <sup>-1</sup> )	WDEs		WBs		ERs	
			Mean (ft)	Std Dev (ft)	Mean (ft)	Std Dev (ft)	Mean (ft)	Std Dev (ft)
1	0.083	3x10 <sup>-5</sup>	4933.2	0.006	4936.5	0.001	<b>4938.7</b>	<b>0.013</b>
2	0.083	3x10 <sup>-6</sup>	4933.2	0.007	4936.5	0.001	<b>4938.7</b>	<b>0.014</b>
3	0.083	3x10 <sup>-7</sup>	4933.2	0.007	4936.5	0.001	<b>4938.7</b>	<b>0.014</b>
4	0.417	3x10 <sup>-5</sup>	4933.1	0.065	4936.4	0.046	<b>4938.6</b>	<b>0.014</b>
5	0.417	3x10 <sup>-6</sup>	4933.1	0.066	4936.4	0.047	<b>4938.6</b>	<b>0.014</b>
6	0.417	3x10 <sup>-7</sup>	4933.1	0.066	4936.4	0.047	<b>4938.6</b>	<b>0.014</b>
7	2.042	3x10 <sup>-5</sup>	4932.5	0.331	4935.9	0.287	<b>4938.3</b>	<b>0.190</b>
8	2.042	3x10 <sup>-6</sup>	4932.5	0.332	4935.9	0.288	<b>4938.3</b>	<b>0.192</b>
9	2.042	3x10 <sup>-7</sup>	4932.5	0.332	4935.9	0.289	<b>4938.3</b>	<b>0.192</b>
10	3.75	3x10 <sup>-5</sup>	4932.4	0.415	4935.7	0.372	<b>4938.2</b>	<b>0.294</b>
11	3.75	3x10 <sup>-6</sup>	4932.4	0.417	4935.7	0.375	<b>4938.2</b>	<b>0.298</b>
12	3.75	3x10 <sup>-7</sup>	4932.4	0.417	4935.7	0.375	<b>4938.2</b>	<b>0.298</b>
13	10	3x10 <sup>-5</sup>	4933.3	0.458	4936.6	0.460	<b>4938.9</b>	<b>0.466</b>
14	10	3x10 <sup>-6</sup>	4933.7	0.476	4937.0	0.478	<b>4939.1</b>	<b>0.482</b>
15	10	3x10 <sup>-7</sup>	4933.6	0.479	4936.8	0.480	<b>4939.0</b>	<b>0.484</b>
16	15	3x10 <sup>-5</sup>	4933.7	0.472	4937.0	0.473	<b>4939.1</b>	<b>0.478</b>
17	15	3x10 <sup>-6</sup>	4933.7	0.483	4937.0	0.485	<b>4939.1</b>	<b>0.488</b>
18	15	3x10 <sup>-7</sup>	4933.6	0.485	4936.8	0.487	<b>4939.0</b>	<b>0.490</b>
19	20	3x10 <sup>-5</sup>	4933.7	0.479	4937.0	0.480	<b>4939.1</b>	<b>0.484</b>
20	20	3x10 <sup>-6</sup>	4933.7	0.488	4936.9	0.489	<b>4939.1</b>	<b>0.493</b>
21	20	3x10 <sup>-7</sup>	4933.6	0.490	4936.8	0.491	<b>4939.0</b>	<b>0.494</b>

The mid piezometer average and standard deviation values range from 4934.61 ft asl to 4938.69 ft asl and 0.006 to 0.496, respectively. Similarly to the shallow piezometers, lower bulk hydraulic conductivity values generally lead to lower average and standard deviation values and higher bulk hydraulic conductivity values generally lead to higher average and standard deviation values. Changes in specific storage appear to have less influence on the model scenario average and standard deviation values than changes to the bulk hydraulic conductivity values.

**Table 8.2: Average and standard deviation values for the homogenous subsurface models, the mid piezometer locations are shown in the table.**

Model Number	Bulk Hydraulic Conductivity (ft/hr)	Specific Storage (ft <sup>-1</sup> )	WRm		EDWm	
			Mean (ft)	Std Dev (ft)	Mean (ft)	Std Dev (ft)
1	0.083	3x10 <sup>-5</sup>	4938.2	0.006	4934.9	0.015
2	0.083	3x10 <sup>-6</sup>	4938.2	0.006	4934.9	0.015
3	0.083	3x10 <sup>-7</sup>	4938.2	0.006	4934.9	0.015
4	0.417	3x10 <sup>-5</sup>	4938.1	0.035	4934.8	0.031
5	0.417	3x10 <sup>-6</sup>	4938.1	0.036	4934.8	0.031
6	0.417	3x10 <sup>-7</sup>	4938.1	0.036	4934.8	0.031
7	2.042	3x10 <sup>-5</sup>	4937.6	0.257	4934.6	0.168
8	2.042	3x10 <sup>-6</sup>	4937.6	0.258	4934.6	0.171
9	2.042	3x10 <sup>-7</sup>	4937.6	0.258	4934.6	0.171
10	3.75	3x10 <sup>-5</sup>	4937.5	0.346	4934.6	0.280
11	3.75	3x10 <sup>-6</sup>	4937.5	0.348	4934.6	0.283
12	3.75	3x10 <sup>-7</sup>	4937.5	0.349	4934.6	0.284
13	10	3x10 <sup>-5</sup>	4938.3	0.461	4935.1	0.472
14	10	3x10 <sup>-6</sup>	4938.6	0.479	4935.3	0.486
15	10	3x10 <sup>-7</sup>	4938.5	0.481	4935.2	0.488
16	15	3x10 <sup>-5</sup>	4938.6	0.474	4935.3	0.482
17	15	3x10 <sup>-6</sup>	4938.6	0.485	4935.3	0.491
18	15	3x10 <sup>-7</sup>	4938.5	0.487	4935.2	0.493
19	20	3x10 <sup>-5</sup>	4938.6	0.481	4935.3	0.488
20	20	3x10 <sup>-6</sup>	4938.6	0.490	4935.3	0.495
21	20	3x10 <sup>-7</sup>	4938.5	0.491	4935.2	0.496

The deep piezometer average and standard deviation values range from 4935.39 ft asl to 4936.86 ft asl and 0.001 to 0.495, respectively. Similarly to the shallow and mid piezometers, lower bulk hydraulic conductivity values generally lead lower average and standard deviation values and higher bulk hydraulic conductivity values generally lead to higher average and standard deviation values. Changes in specific storage appear to have less influence on the model scenario average and standard deviation values than changes to the bulk hydraulic conductivity values.

Additionally, a spatial comparison can be made between the east and west piezometer nests. The eastern piezometer nests show less variation in calculated average values than the western piezometers for all depth regimes. The range of standard deviation values remains

relatively constant with varying distance from the river, depth regime, and piezometer location (east or west of the river).

**Table 8.3: Average and standard deviation values for the homogenous subsurface model case, the deep piezometer locations are shown in the table.**

Model Number	Bulk Hydraulic Conductivity (ft/hr)	Specific Storage (ft <sup>-1</sup> )	WBd		EBd	
			Mean (ft)	Std Dev (ft)	Mean (ft)	Std Dev (ft)
1	0.083	3x10 <sup>-5</sup>	4936.1	0.001	<b>4936.3</b>	<b>0.014</b>
2	0.083	3x10 <sup>-6</sup>	4936.1	0.001	<b>4936.3</b>	<b>0.014</b>
3	0.083	3x10 <sup>-7</sup>	4936.1	0.001	<b>4936.3</b>	<b>0.014</b>
4	0.417	3x10 <sup>-5</sup>	4936.0	0.046	<b>4936.3</b>	<b>0.017</b>
5	0.417	3x10 <sup>-6</sup>	4936.0	0.047	<b>4936.3</b>	<b>0.017</b>
6	0.417	3x10 <sup>-7</sup>	4936.0	0.047	<b>4936.3</b>	<b>0.017</b>
7	2.042	3x10 <sup>-5</sup>	4935.5	0.287	<b>4936.0</b>	<b>0.176</b>
8	2.042	3x10 <sup>-6</sup>	4935.5	0.288	<b>4936.0</b>	<b>0.178</b>
9	2.042	3x10 <sup>-7</sup>	4935.5	0.289	<b>4936.0</b>	<b>0.178</b>
10	3.75	3x10 <sup>-5</sup>	4935.3	0.372	<b>4935.9</b>	<b>0.285</b>
11	3.75	3x10 <sup>-6</sup>	4935.3	0.375	<b>4935.9</b>	<b>0.288</b>
12	3.75	3x10 <sup>-7</sup>	4935.3	0.375	<b>4935.9</b>	<b>0.289</b>
13	10	3x10 <sup>-5</sup>	4936.2	0.460	<b>4936.6</b>	<b>0.468</b>
14	10	3x10 <sup>-6</sup>	4936.6	0.478	<b>4936.8</b>	<b>0.484</b>
15	10	3x10 <sup>-7</sup>	4936.5	0.480	<b>4936.7</b>	<b>0.486</b>
16	15	3x10 <sup>-5</sup>	4936.6	0.473	<b>4936.8</b>	<b>0.480</b>
17	15	3x10 <sup>-6</sup>	4936.6	0.485	<b>4936.8</b>	<b>0.490</b>
18	15	3x10 <sup>-7</sup>	4936.4	0.487	<b>4936.7</b>	<b>0.491</b>
19	20	3x10 <sup>-5</sup>	4936.6	0.480	<b>4936.8</b>	<b>0.486</b>
20	20	3x10 <sup>-6</sup>	4936.6	0.489	<b>4936.8</b>	<b>0.494</b>
21	20	3x10 <sup>-7</sup>	4936.4	0.491	<b>4936.6</b>	<b>0.495</b>

The calculated average and standard deviation values for the layered subsurface models are shown in Tables 8.4-8.6. Bold values indicate the piezometer is closer to the Rio Grande and italicized values indicate the piezometer is further away from the Rio Grande. The average shallow piezometer values range from 4933.52 ft asl to 4939.19 ft asl. The lowest values were again observed at the WDEs piezometer (furthest piezometer) and the highest values at the ERs piezometer (closest piezometer). The selected shallow piezometer standard deviation values range from 0.362 to 0.471.

Although the hydraulic conductivity for each subsurface type varies between the layered model scenarios, the geometric mean for all layers in each model scenario was 15 ft/hr. As shown in Table 8.4 the calculated average and standard deviation values do not vary greatly between the different layered subsurface modeling scenarios. Again, implying that the hydraulic conductivity more greatly influences the average and standard deviation values than changes in specific storage.

Additionally, the layered subsurface models provide very similar results for the shallow piezometers to the homogenous subsurface of 15 ft/hr bulk hydraulic conductivity (model number 16,17,18) modeling scenarios. A slight increase in standard deviation can be observed as specific storage is decreased for the layered subsurface models.

**Table 8.4: Average and standard deviation values for the layered subsurface model cases, the shallow piezometer locations are shown in the table.**

Model Number	Case Number	Specific Storage (ft <sup>-1</sup> )	WDEs		WBs		ERs	
			Mean (ft)	Std Dev (ft)	Mean (ft)	Std Dev (ft)	Mean (ft)	Std Dev (ft)
22	Case 1	3x10 <sup>-5</sup>	4933.7	0.438	4937.0	0.440	<b>4939.1</b>	<b>0.449</b>
23	Case 1	3x10 <sup>-6</sup>	4933.5	0.448	4936.8	0.451	<b>4939.0</b>	<b>0.458</b>
24	Case 1	3x10 <sup>-7</sup>	4933.6	0.450	4936.8	0.452	<b>4939.0</b>	<b>0.460</b>
25	Case 2	3x10 <sup>-5</sup>	4933.7	0.456	4937.0	0.457	<b>4939.1</b>	<b>0.463</b>
26	Case 2	3x10 <sup>-6</sup>	4933.7	0.464	4936.9	0.465	<b>4939.1</b>	<b>0.470</b>
27	Case 2	3x10 <sup>-7</sup>	4933.5	0.465	4936.7	0.466	<b>4938.9</b>	<b>0.471</b>
28	Case 3	3x10 <sup>-5</sup>	4933.7	0.362	4937.0	0.367	<b>4939.1</b>	<b>0.383</b>
29	Case 3	3x10 <sup>-6</sup>	4933.7	0.368	4936.9	0.372	<b>4939.1</b>	<b>0.387</b>
30	Case 3	3x10 <sup>-7</sup>	4933.5	0.368	4936.8	0.372	<b>4939.0</b>	<b>0.388</b>
31	Case 4	3x10 <sup>-5</sup>	4933.7	0.433	4936.9	0.435	<b>4939.1</b>	<b>0.441</b>
32	Case 4	3x10 <sup>-6</sup>	4933.7	0.439	4936.9	0.441	<b>4939.1</b>	<b>0.446</b>
33	Case 4	3x10 <sup>-7</sup>	4933.6	0.440	4936.9	0.441	<b>4939.0</b>	<b>0.447</b>

The mid piezometer average and standard deviation values ranged from 4935.16 ft asl to 4938.69 ft asl and 0.370 to 0.475, respectively. Similar to the shallow piezometers, the calculated average and standard deviation values do not vary greatly between the different layered subsurface modeling scenarios. Additionally, the layered subsurface models provide very similar results for the mid piezometers to the homogenous subsurface 15 ft/hr bulk hydraulic conductivity (model numbers 16, 17, and 18) modeling scenarios.

**Table 8.5: Average and standard deviation values for the layered subsurface models, the mid piezometer locations are shown in the table.**

Model Number	Case Number	Specific Storage (ft <sup>-1</sup> )	WRm		EDWm	
			Mean (ft)	Std Dev (ft <sup>-1</sup> )	Mean (ft)	Std Dev (ft)
22	Case 1	3x10 <sup>-5</sup>	<b>4938.6</b>	<b>0.442</b>	<i>4935.3</i>	<i>0.456</i>
23	Case 1	3x10 <sup>-6</sup>	<b>4938.5</b>	<b>0.452</b>	<i>4935.2</i>	<i>0.464</i>
24	Case 1	3x10 <sup>-7</sup>	<b>4938.5</b>	<b>0.454</b>	<i>4935.2</i>	<i>0.466</i>
25	Case 2	3x10 <sup>-5</sup>	<b>4938.6</b>	<b>0.459</b>	<i>4935.3</i>	<i>0.467</i>
26	Case 2	3x10 <sup>-6</sup>	<b>4938.6</b>	<b>0.466</b>	<i>4935.3</i>	<i>0.474</i>
27	Case 2	3x10 <sup>-7</sup>	<b>4938.4</b>	<b>0.467</b>	<i>4935.1</i>	<i>0.475</i>
28	Case 3	3x10 <sup>-5</sup>	<b>4938.6</b>	<b>0.370</b>	<i>4935.3</i>	<i>0.396</i>
29	Case 3	3x10 <sup>-6</sup>	<b>4938.6</b>	<b>0.375</b>	<i>4935.3</i>	<i>0.400</i>
30	Case 3	3x10 <sup>-7</sup>	<b>4938.5</b>	<b>0.376</b>	<i>4935.2</i>	<i>0.400</i>
31	Case 4	3x10 <sup>-5</sup>	<b>4938.6</b>	<b>0.436</b>	<i>4935.3</i>	<i>0.445</i>
32	Case 4	3x10 <sup>-6</sup>	<b>4938.6</b>	<b>0.442</b>	<i>4935.3</i>	<i>0.451</i>
33	Case 4	3x10 <sup>-7</sup>	<b>4938.5</b>	<b>0.443</b>	<i>4935.2</i>	<i>0.451</i>

The deep piezometer average and standard deviation values range from 4936.40 ft asl to 4936.86 ft asl and 0.367 to 0.473, respectively. Unlike to the shallow and mid piezometers, the calculated standard deviation values appear to vary between the different layered subsurface modeling scenarios even though the geometric mean hydraulic conductivity is constants for all the layered subsurface model scenarios.

The calculated average and standard deviation values for the random field subsurface models are shown in Tables 8.7-8.9. Bold values indicate the piezometer is closer to the Rio Grande and italicized values indicate the piezometer is further from the Rio Grande. The average shallow piezometer values range from 4933.63 ft asl to 4939.19 ft asl. The lowest values were again observed at the WDEs piezometer (furthest piezometer) and the highest values at the ERs piezometer (closest piezometer). The selected shallow piezometer standard deviation values range from 0.489 to 0.508.

**Table 8.6: Average and standard deviation values for the layered subsurface models, the deep piezometer locations are shown in the table.**

Model Number	Case Number	Specific Storage (ft <sup>-1</sup> )	WBd		EBd	
			Mean (ft)	Std Dev (ft)	Mean (ft)	Std Dev (ft)
22	Case 1	3x10 <sup>-5</sup>	4936.6	0.440	<b>4936.8</b>	<b>0.452</b>
23	Case 1	3x10 <sup>-6</sup>	4936.4	0.451	<b>4936.6</b>	<b>0.461</b>
24	Case 1	3x10 <sup>-7</sup>	4936.4	0.452	<b>4936.7</b>	<b>0.462</b>
25	Case 2	3x10 <sup>-5</sup>	4936.6	0.457	<b>4936.8</b>	<b>0.464</b>
26	Case 2	3x10 <sup>-6</sup>	4936.6	0.465	<b>4936.8</b>	<b>0.472</b>
27	Case 2	3x10 <sup>-7</sup>	4936.4	0.466	<b>4936.6</b>	<b>0.473</b>
28	Case 3	3x10 <sup>-5</sup>	4936.6	0.367	<b>4936.8</b>	<b>0.388</b>
29	Case 3	3x10 <sup>-6</sup>	4936.6	0.372	<b>4936.7</b>	<b>0.393</b>
30	Case 3	3x10 <sup>-7</sup>	4936.4	0.372	<b>4936.6</b>	<b>0.393</b>
31	Case 4	3x10 <sup>-5</sup>	4936.6	0.435	<b>4936.8</b>	<b>0.443</b>
32	Case 4	3x10 <sup>-6</sup>	4936.6	0.441	<b>4936.8</b>	<b>0.448</b>
33	Case 4	3x10 <sup>-7</sup>	4936.54	0.441	<b>4936.7</b>	<b>0.449</b>

The random field subsurface realizations were generated in ParFlow using a correlated, Gaussian random field approach via the Turning Bands method (Tompson et al 1989), where a permeability value is assigned to each node within the domain. The entire model domain has a geometric mean of 15 ft/hr.

As can be observed, the calculated average and standard deviation values do not vary greatly between the different random field subsurface modeling scenarios. This again suggests that the hydraulic conductivity influences the average and standard deviation values more than changes in the specific storage. Additionally, the random field subsurface models provide very similar results for the shallow piezometers to the homogenous subsurface 15 ft/hr bulk hydraulic conductivity and layered subsurface modeling scenarios. The 3.048 x 10<sup>-7</sup> ft<sup>-1</sup> specific storage, random field model leads to the largest observed standard deviations for all the model scenarios.

**Table 8.7: Average and standard deviation value for the Random Field subsurface models, the shallow piezometer locations are shown in the table.**

Model Number	Specific Storage (ft <sup>-1</sup> )	WDEs		WBs		ERs	
		Mean (ft)	Std Dev (ft)	Mean (ft)	Std Dev (ft)	Mean (ft)	Std Dev (ft)
34	3x10 <sup>-5</sup>	4933.7	0.489	4937.0	0.489	<b>4939.1</b>	<b>0.493</b>
35	3x10 <sup>-6</sup>	4933.7	0.503	4937.0	0.504	<b>4939.1</b>	<b>0.506</b>
36	3x10 <sup>-7</sup>	4933.6	0.506	4936.8	0.506	<b>4939.0</b>	<b>0.508</b>

The mid piezometer average and standard deviation values ranged from 4935.23 ft asl to 4938.68 ft asl and 0.490 to 0.509, respectively. Similar to the shallow piezometers, the calculated average values do not vary greatly between the different random field subsurface modeling scenarios. Additionally, the random field subsurface models provide very similar results to the mid piezometers to the homogenous subsurface 15 ft/hr bulk hydraulic conductivity and layered subsurface modeling scenarios.

**Table 8.8: Average and standard deviation values for the random field subsurface models, the mid piezometer locations are shown in the table.**

Model Number	Specific Storage (ft <sup>-1</sup> )	WRm		EDWm	
		Mean (ft)	Std Dev (ft)	Mean (ft)	Std Dev (ft)
34	3x10 <sup>-5</sup>	<b>4938.6</b>	<b>0.490</b>	4935.3	0.496
35	3x10 <sup>-6</sup>	<b>4938.6</b>	<b>0.504</b>	4935.3	0.507
36	3x10 <sup>-7</sup>	<b>4938.5</b>	<b>0.506</b>	4935.2	0.509

The deep piezometer average and standard deviation values range from 4936.50 ft asl to 4936.86 ft asl and 0.489 to 0.508, respectively. Similar to the shallow and mid piezometers, the calculated average values do not vary greatly between the different random field subsurface modeling scenarios and provide very similar results for the deep piezometers to the homogenous subsurface 15 ft/hr bulk hydraulic conductivity and layered subsurface modeling scenarios.

**Table 8.9: Average and standard deviation values for the random field subsurface models, the deep piezometer locations are shown in the table.**

Model Number	Specific Storage (ft <sup>-1</sup> )	<i>WBd</i>		<b>EBd</b>	
		<i>Mean (ft)</i>	<i>Std Dev (ft)</i>	<b>Mean (ft)</b>	<b>Std Dev (ft)</b>
34	3x10 <sup>-5</sup>	4936.6	0.489	<b>4936.8</b>	<b>0.494</b>
35	3x10 <sup>-6</sup>	4936.6	0.504	<b>4936.8</b>	<b>0.506</b>
36	3x10 <sup>-7</sup>	4936.5	0.506	<b>4936.7</b>	<b>0.508</b>

As expected, by increasing variability in the model subsurface representation, there is an observable increase in the maximum standard deviation between the homogenous subsurface, layered subsurface, and random field subsurface models. In contrast, increasing the variability in the model subsurface representation does not significantly change the calculated average values.

## 8.2 Numerical Model Scenario Comparison Plots

All of the Parflow model results are analyzed in comparison with the observed values for each piezometer location in order to qualitatively assess model fit. The shallow, mid, and deep piezometers are shown on separate plots, where the shallow piezometer plot includes subplots for the WDE, WB, WR, ER, EB, and EDW shallow piezometers and the Rio Grande, the mid piezometer plot included subplots for the WR and EDW mid piezometers and the Rio Grande and the deep piezometer plot included subplots for the WB and EB deep piezometers. Appendix A contains all of the individual model scenario plots. Appendix C contains all of the comparison plots.

A series of plots were created comparing the different hydraulic conductivity and specific storage values used in the model scenarios. These analyses are separated into two categories: 1) plots where the specific storage is kept constant and the hydraulic conductivity varied and 2) plots where the hydraulic conductivity is kept constant and the specific storage is varied.

Figure 8.1 shows the 2006-2007 water year model results for a subset of the homogenous subsurface models for the shallow piezometer locations. Three piezometer locations, the WDE piezometer (furthest piezometer from the river), the WB piezometer (mid distance to the river), and the ER piezometer (closest to the river), are compared for the observed values (in black), 0.417 ft/hr (in green), 2.042 hr/ft (in yellow), 3.750 ft/hr (in blue), and 15 ft/hr (in red) bulk

hydraulic conductivity models. As shown in Figure 8.1, model fit appears to be related to distance from the river. In order to further investigate the spatial relationship of model fit, a three-month section of the data is shown separately for closer inspection.

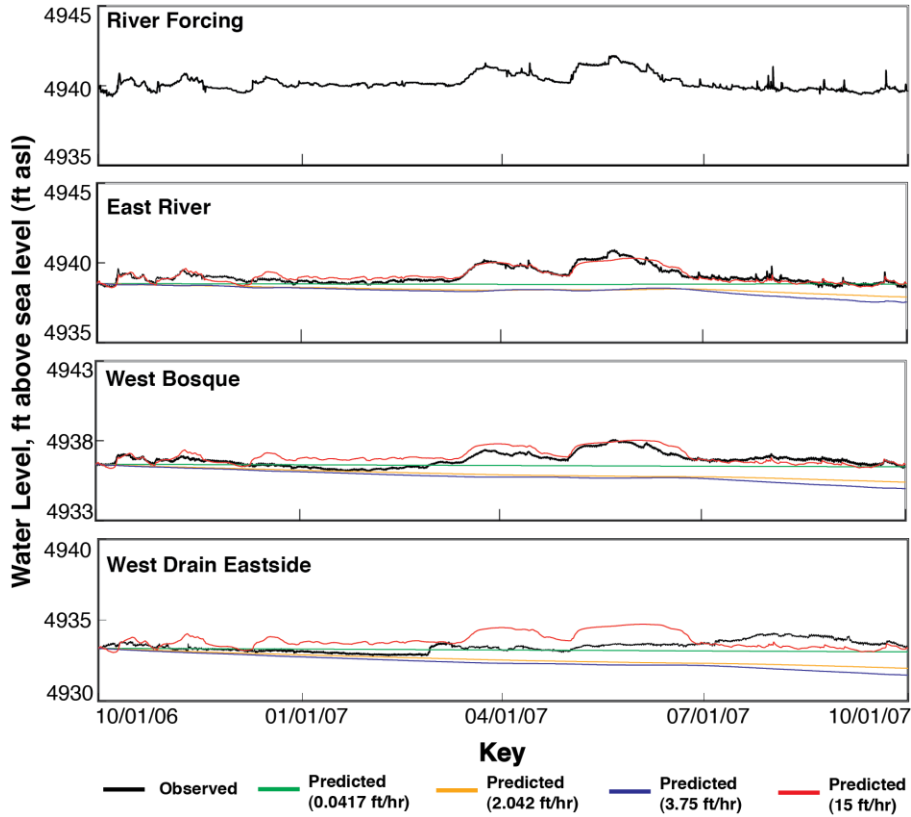


**Figure 8.1: Comparison of four homogenous subsurface model scenarios, the shallow piezometer locations are shown in the figure.**

Figure 8.2 shows the simulated water table elevation for the shallow piezometer locations for the months of April, May, and June 2007. During this three-month period, there is a rise in the Rio Grande stage from base flow to peak flow followed by a subsequent return to baseflow, which occurs over roughly a month and a half. The observed values for the WDE, WB, and ER show three very different responses to the change in river signal. The ER piezometer tracks the rise and fall of the river stage closely, whereas the WDE piezometer's response is a dampened and slightly lagged version of the river signal.

Examining the numerical model predicted values, it is clear that each bulk hydraulic conductivity model scenario provides a different piezometer signal for the three piezometer locations. The 15 ft/hr bulk hydraulic conductivity model matches the ER piezometer signal well, but tends to overestimate WB piezometer signal some and WDE piezometer signals for the entire three-month period. The 2.042 and 3.750 ft/hr bulk hydraulic conductivity models underestimate the all the piezometer signals. The 0.417 ft/hr bulk hydraulic conductivity matches the WDE piezometer signal well, although still underestimating the signal slightly.

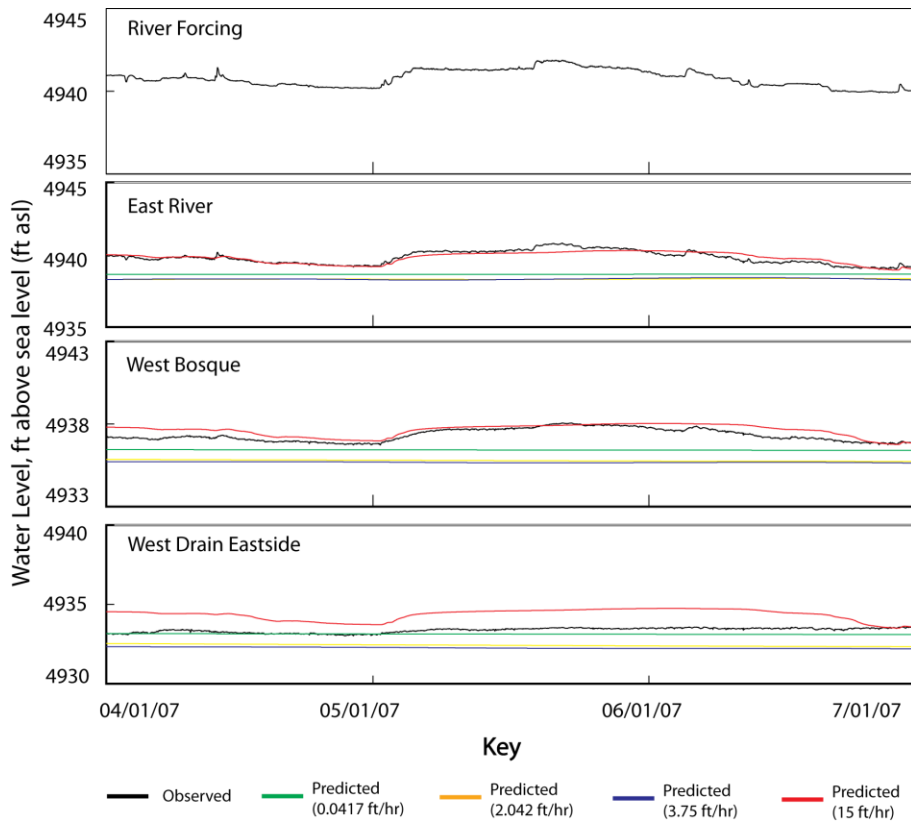


**Figure 8.2: Comparison of four homogenous subsurface model scenarios from April 2007 to June 2007, the shallow piezometer locations.**

Figure 8.3 shows the simulated water table elevation for the mid piezometer locations for the months of April, May, and June 2007. Like the shallow piezometers, the response of the mid piezometers to changes in river stage appears to be a function of piezometer distance from the river. The WR piezometer (closer piezometer) signal follows closely the changes in the river signal, whereas the EDW piezometer (more distant piezometer) has a more dampened and

slightly lagged signal. Although each piezometer responds similarly to the shallow piezometer's observed signals, the model predicted values do not match as well in either case. The 15 ft/hr. homogenous subsurface model case underestimates the rise observed at the WRm piezometer and subsequently overestimates its return to base flow. The 15 ft/hr homogenous subsurface model case overestimates the entire period for the EDWm piezometer. The other three model cases underestimate the observed values for both piezometers for the entire three-month period.

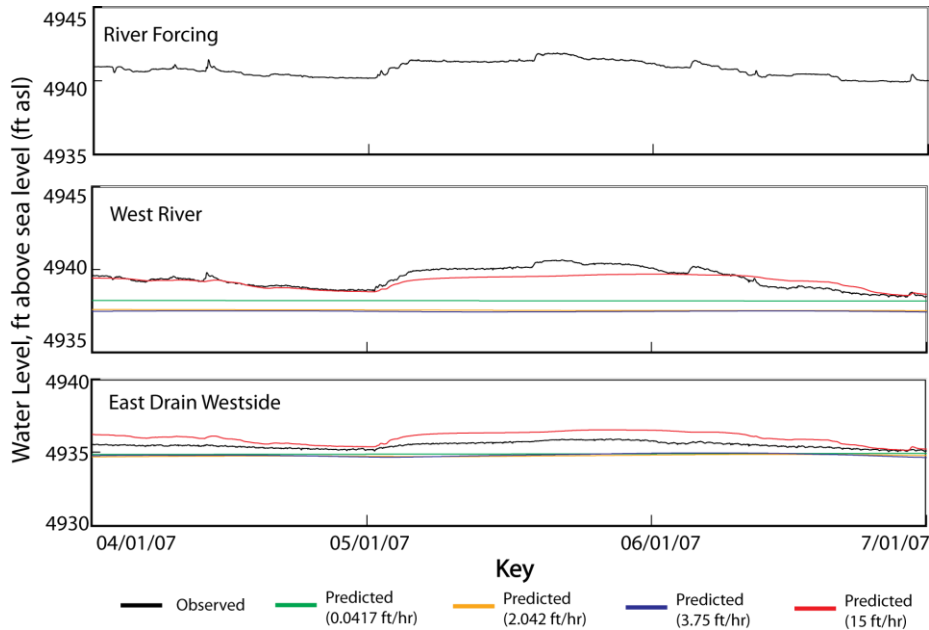
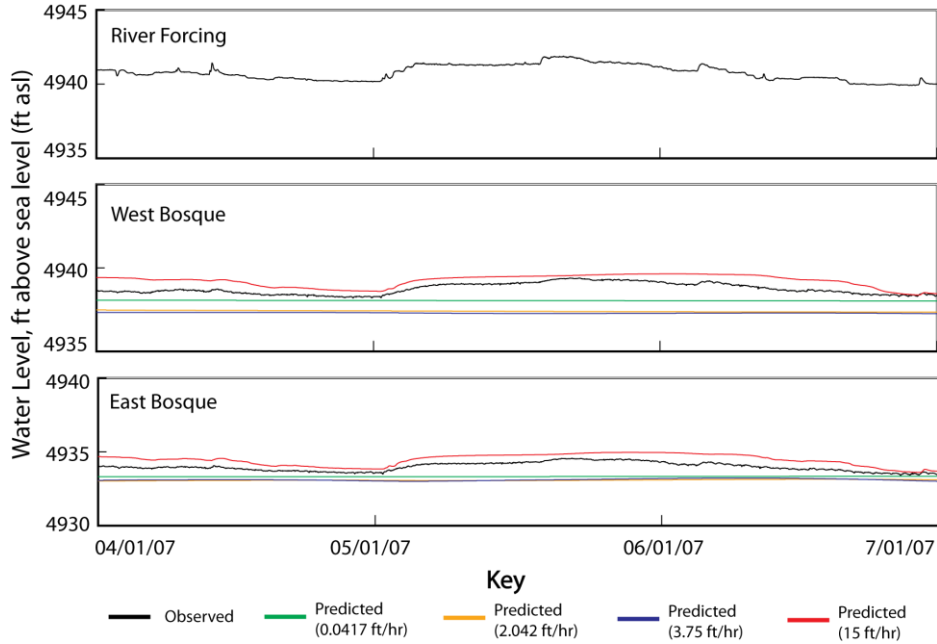


**Figure 8.3: Comparison of four homogenous subsurface model from April to June 2007, the mid piezometer locations are shown in the figure.**

Figure 8.4 shows the simulated water table elevation for the deep piezometer locations for the months of April, May, and June 2007. The WBd and EBd piezometers observed values rise and fall with the rise and fall of the river. Both signals show some dampening and a short lag period.

In the case of the deep piezometers, the 15 ft/hr bulk hydraulic conductivity model overestimates the piezometer signal while the other three model cases underestimate the observed values. This suggests that model fit is affected by distance from the river as well as piezometer depth. As the piezometer depth increases the higher hydraulic conductivity model tends to overestimate, while the low bulk hydraulic conductivity models continue to underestimate. Thus

dampening of the river signal is related to both distance from the river and the depth of the piezometer, suggesting horizontal and vertical anisotropy within in the natural system.



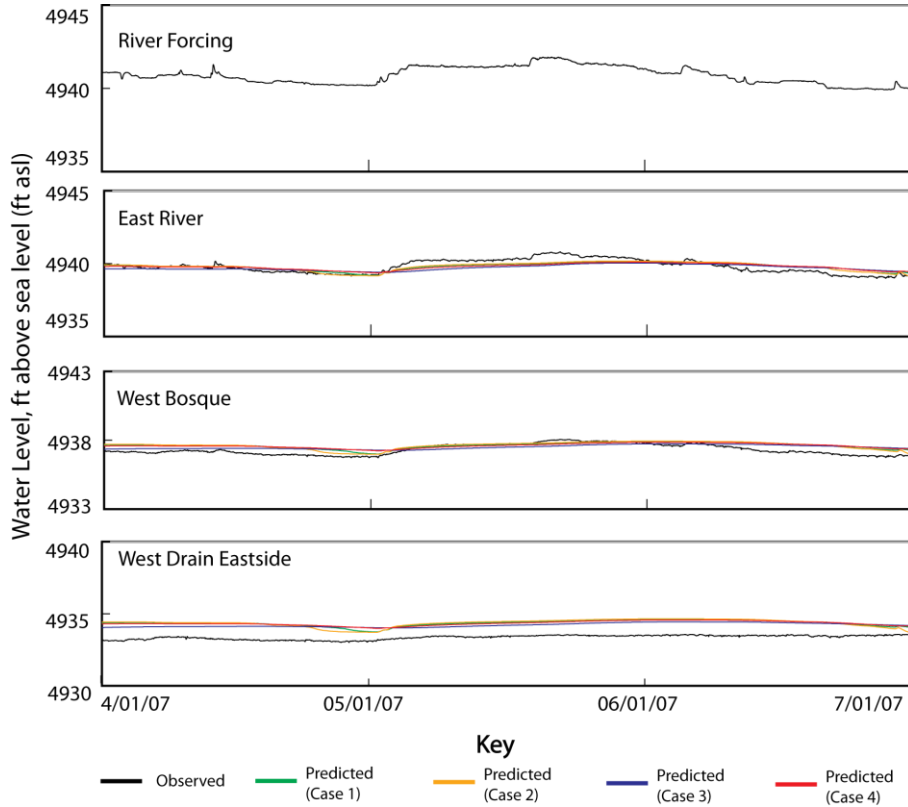
**Figure 8.4: Comparison of four homogenous subsurface model scenarios for April to June 2007, the deep piezometer locations.**

Figure 8.5 shows the simulated water table elevation for the layered subsurface model cases at the shallow piezometers for the months of April, May, and June 2007. The WDE piezometer, the WB piezometer, and the ER piezometer were compared for the observed values (in black), Case 1 (in green), Case 2 (in yellow), Case 3 (in blue), and Case 4 (in red) layered models assuming a specific storage of  $3.048 \times 10^{-5}$ .

Although the hydraulic conductivity for each sediment type varied between the layered subsurface model scenarios, they all maintained a geometric mean of 15 ft/hr for the domain. Figure 8.5 shows that the sediment hydraulic conductivities did not strongly affect the model response to changes in river signal. All of the layered subsurface model scenarios responded in the same manner to changes in the river signal, increasing and decreasing in unison.

Additionally, the layered subsurface models have a similar response to the 15 ft/hr homogenous subsurface models. Like the 15 ft/hr homogenous subsurface model, the layered subsurface model's predicted values agree reasonably well with the observed values of the ER

and WB piezometers and overestimate the WDE piezometer signal. Unlike the 15 ft/hr homogenous models, the layered subsurface models overestimate base flow and underestimate peak flow for the ER and WB piezometers.



**Figure 8.5: Comparison of four layered subsurface model scenario for April to June 2007, the shallow piezometer locations.**

It was observed for the Barelax Cross-section’s natural system as piezometer depth increased the observed piezometer signal became dampened from the river signal and slightly lagged. The homogenous subsurface models do not have sufficient subsurface characterization to effectively represent the deeper piezometer observed values. It can be hypothesized that improved characterization of the subsurface would improve model fit.

Figure 8.6 shows the simulated water table elevation for the layered subsurface model cases at the mid piezometer locations for the months of April, May, and June 2007. The layered subsurface models increased dampening of the river signal for the deeper piezometers in

comparison to the homogenous subsurface models, which improved the model fit at the EDWm piezometer, but weakened the model fit at the WRm piezometer.

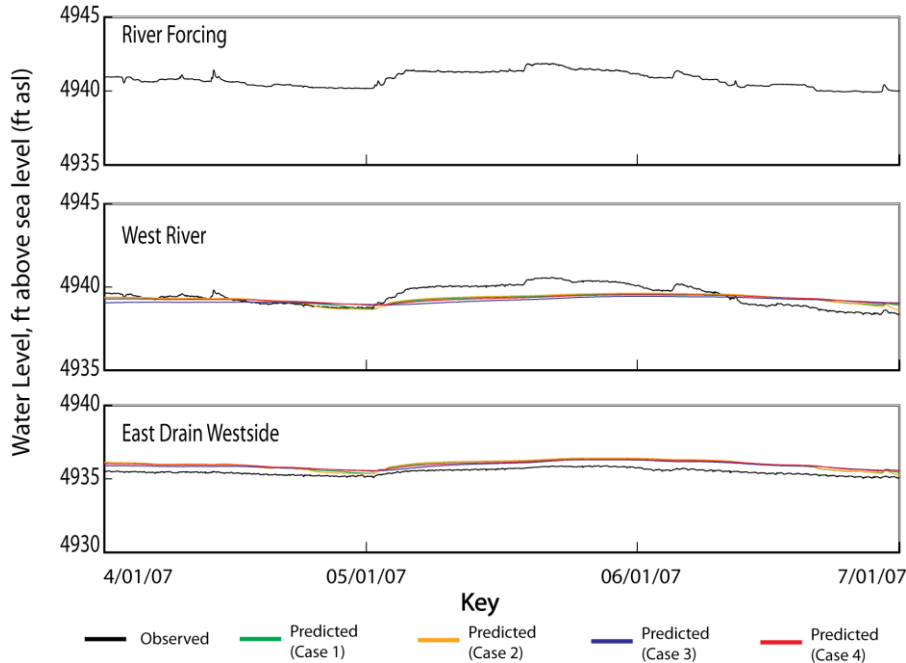


**Figure 8.6: Comparison of four layered subsurface model scenario for April to June 2007, the mid piezometer locations.**

Figure 8.7 shows the simulated water table elevation for the 15 ft/hr homogenous subsurface model cases for the months of July, August, and September 2007. Three shallow piezometer locations were selected for comparison: the WDE piezometer, the WB piezometer, and the ER piezometer. Figure 8.7 is comparing different specific storage values, where the observed values are in black, the  $3.048 \times 10^{-5} \text{ ft}^{-1}$  specific storage model case is in blue, the  $3.048 \times 10^{-6} \text{ ft}^{-1}$  specific storage model case is in green, the  $3.048 \times 10^{-7} \text{ ft}^{-1}$  specific storage model case is in red.

During the July to September three-month period, the Rio Grande stage shows a series of high frequency short duration peaks, which likely correspond to summer monsoon storm events. The observed values for the WDE, WB, and ER piezometer locations show a dampened response to the change in river signal. Signal dampening increases with increasing distance from the river, thus signal dampening is stronger at the WDE piezometer location than at the ER piezometer location.

Changing the specific storage value does not appear to greatly affect model fit. The three specific storage models maintain the same predicted trends. However, decreasing the specific storage does appear to affect how many of the high frequency river changes are predicted by the numerical model at the piezometer locations. The  $3.048 \times 10^{-7} \text{ ft}^{-1}$  model predicts more high frequency values than the  $3.048 \times 10^{-5} \text{ ft}^{-1}$  model.

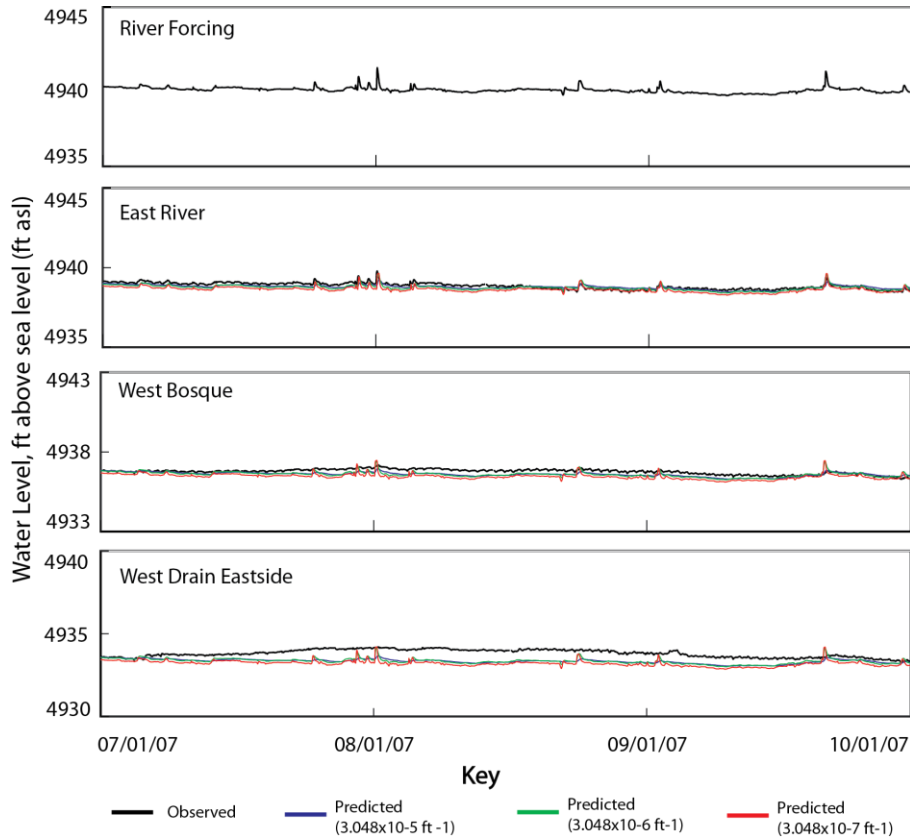


**Figure 8.7: Comparison of specific storage for 15 ft/hr bulk hydraulic conductivity homogenous subsurface models, the shallow piezometer locations.**

Figure 8.8 shows the simulate water table elevation for the Case 1 layered subsurface models for the months of July, August and September 2007. Three shallow piezometer locations were chosen for comparison: the WDE piezometer, the WB piezometer, and the ER piezometer. Figure 8.8 compares specific storage values, where the observed values are in black, the  $3.048 \times 10^{-5} \text{ ft}^{-1}$  specific storage model case is in blue, the  $3.048 \times 10^{-6} \text{ ft}^{-1}$  specific storage model case is in green, and the  $3.048 \times 10^{-7} \text{ ft}^{-1}$  specific storage model case is in red.

The Case 1 layered subsurface models responds very similarly to the 15ft/hr bulk hydraulic conductivity homogenous subsurface models. Like the homogenous subsurface model cases, changing the specific storage value in the layered model cases does not appear to greatly affect the model fit, but decreasing the specific storage increases the number of high frequency events predicted by at the piezometer locations.

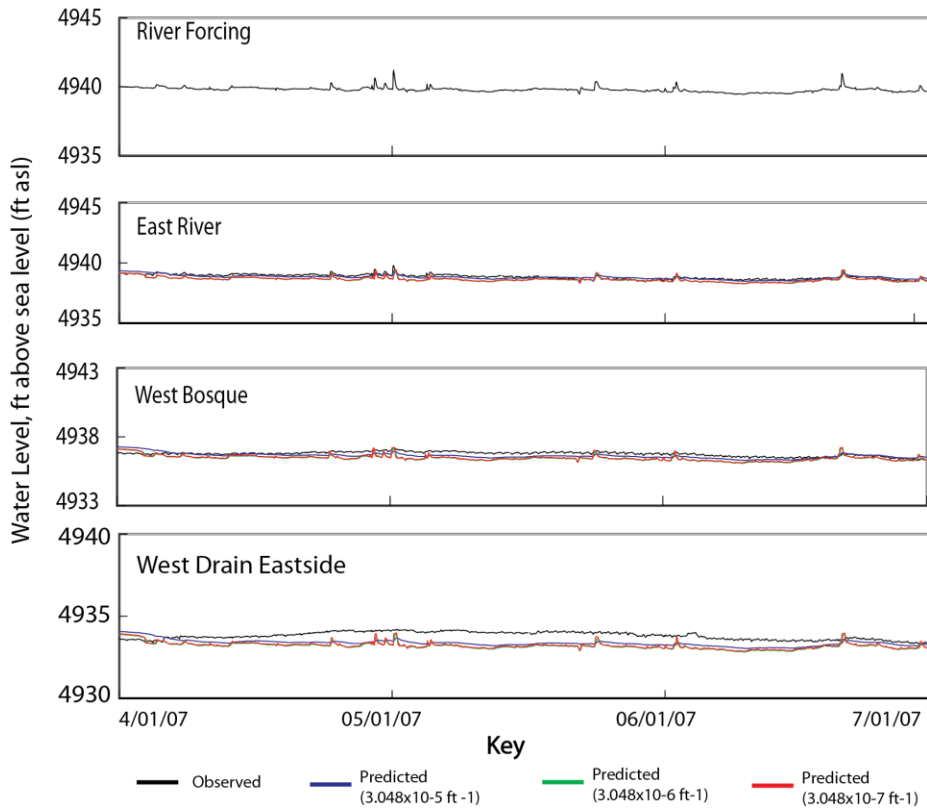


**Figure 8. 8: Comparison of specific storage for Case 1 layered subsurface models, the shallow piezometer locations.**

Figure 8.9 shows the simulated water table elevation for the random field subsurface models for the months of July, August, and September 2007. Three shallow piezometer locations were compared: the WDE piezometer, the WB piezometer, and the ER piezometer. Figure 8.8 compares specific storage values, where the observed values are in black, the  $3.048 \times 10^{-5} \text{ ft}^{-1}$  specific storage model case is in blue, the  $3.048 \times 10^{-6} \text{ ft}^{-1}$  specific storage model case is in green, and the  $3.048 \times 10^{-7} \text{ ft}^{-1}$  specific storage model case is in red.

The random field subsurface model cases respond very similarly to the 15ft/hr bulk hydraulic conductivity homogenous subsurface and Case 1 layered subsurface models. Changing the specific storage value used did not appear to greatly affect the model fit, but decreasing the specific storage value appears to increase the amount of high frequency events predicted by the numerical model.

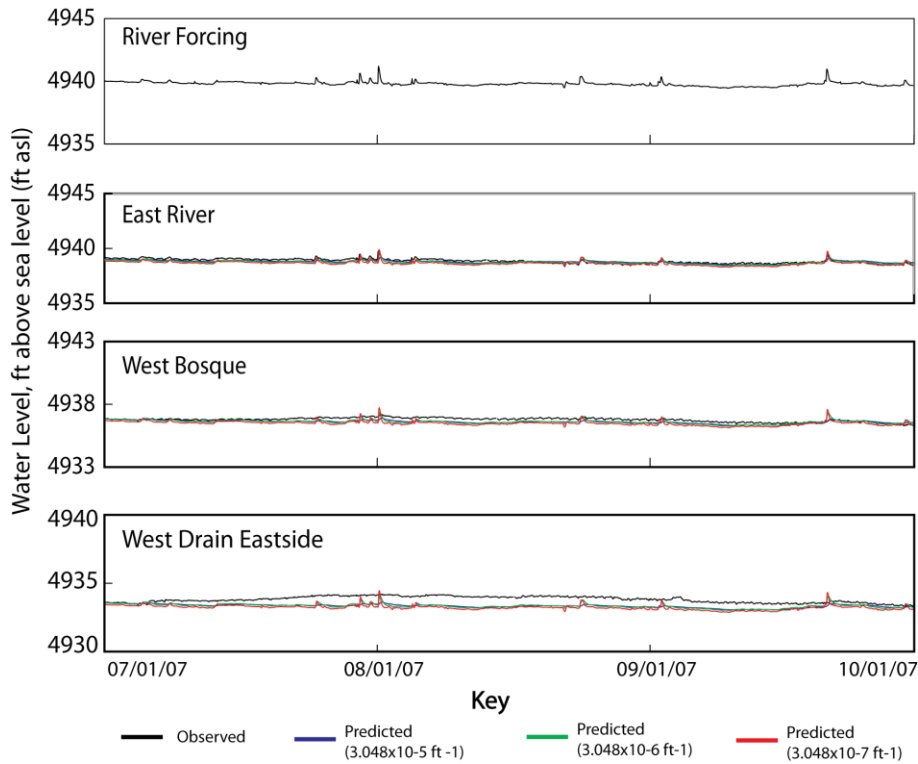


**Figure 8.9: Comparison of specific storage for random field subsurface models, the shallow piezometer locations.**

### 8.3 Observed vs. Predicted Values Plots

The observed and predicted values for each piezometer location are shown as scatterplots in order to quantitatively assess model fit. Figures 8.10-8.12 compare the observed values to the predicted values from the 0.417 ft/hr, 3.750 ft/hr, and 15 ft/hr bulk hydraulic conductivity homogenous subsurface model cases for all piezometer locations. Here, the shallow piezometers are represented by dots, the mid piezometers by stars, the deep piezometers by xs, the one-to-one fit line by a dashed black line, and the linear regression line by a solid black line. In the

scatterplot, values below the one-to-one line indicate an underestimation of the observed value and values above the one-to-one line indicate an overestimation of the observed value.

As shown in Figure 8.10, the 0.417 ft/hr bulk hydraulic conductivity homogenous subsurface model predicted values do not agree well with the observed values for any of the piezometer locations. The model underestimated most of the values, but a spatial relationship between model prediction and piezometer distance from the river can still be observed. The ER and WR piezometers were mostly underestimated while the EDW piezometers are mostly overestimated. The  $R^2$  value for the linear regression is 0.88.

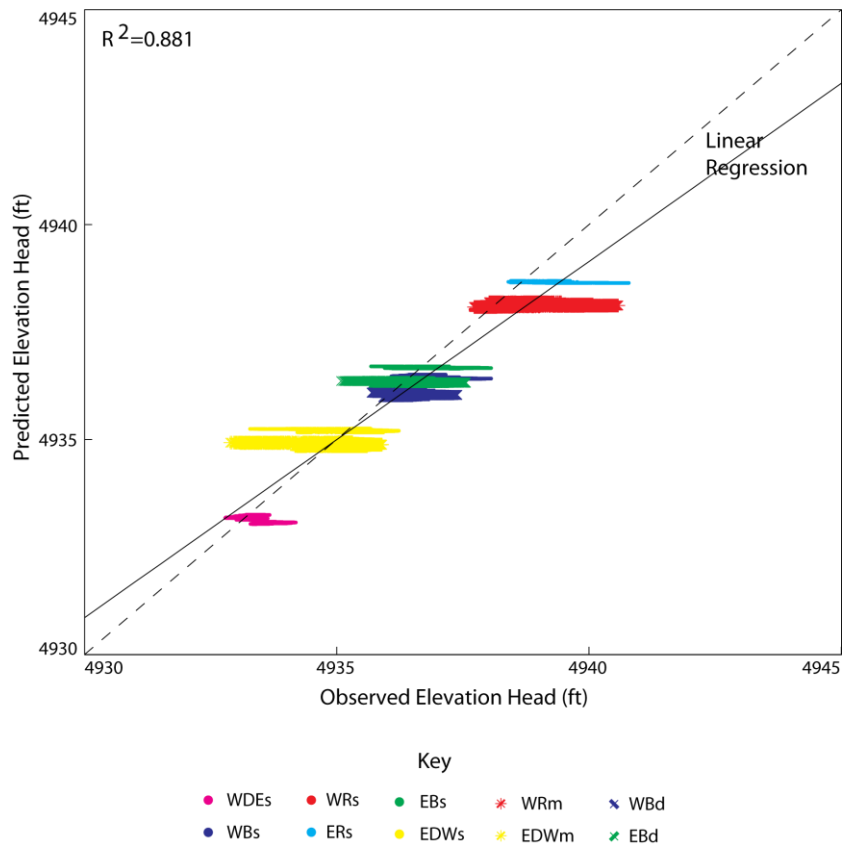


**Figure 8.10: Plot of predicted vs. observed values of water table elevation for 0.417 ft/hr homogenous subsurface model. ( $ss=3.048 \times 10^{-5} \text{ ft}^{-1}$ )**

The 3.750 ft/hr bulk hydraulic conductivity homogenous subsurface model case predicted values are shown in Figure 8.11. Similar to the 0.417 ft/hr bulk hydraulic conductivity homogenous subsurface model case predicted values, the 3.750 ft/hr model case values do not agree well with the observed values for any of the piezometer locations, however the two models

show very different fits. The 3.750 ft/hr model underestimated most of the observed values. The EDW and EB piezometer locations show slightly better fit than the other piezometers for the 3.750 ft/hr model case. The  $R^2$  value for the linear regression is 0.68.

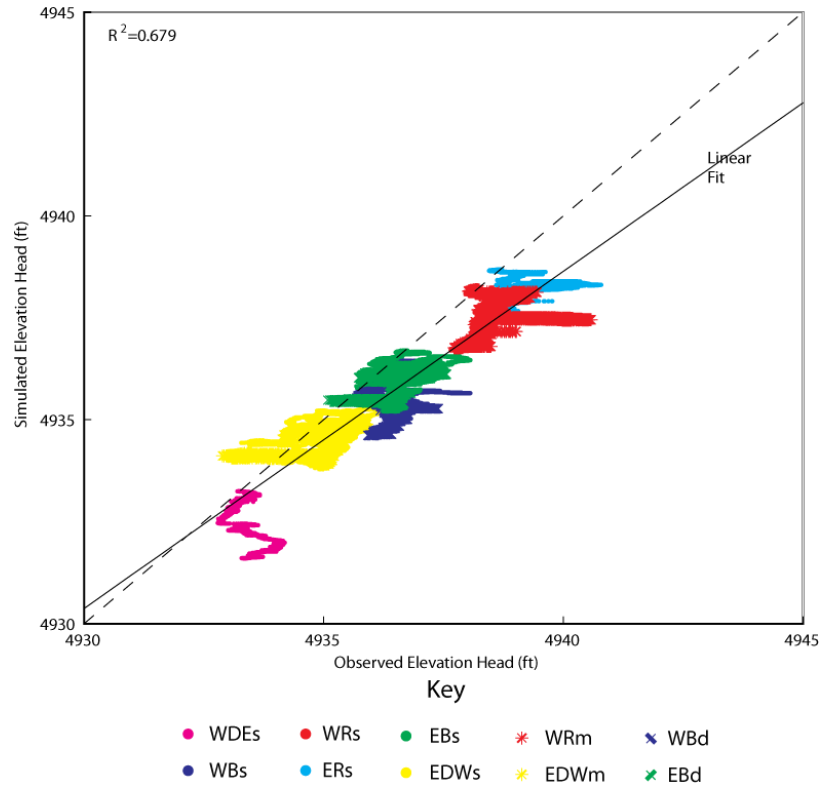


**Figure 8.11: Plot of predicted vs. observed values of water table elevation for 3.750 ft/hr homogenous subsurface model. ( $ss=3.048 \times 10^{-5} \text{ ft}^{-1}$ )**

Figure 8.12 shows a scatterplot of the 15 ft/hr homogenous bulk hydraulic conductivity subsurface model case predicted values. When comparing the 0.417 ft/hr, 3.750 ft/hr, and 15 ft/hr model cases, it can be observed that increasing the bulk hydraulic conductivity improves model fitness. Where the 0.417 and 3.750 ft/hr models underestimate most of the observed values, the 15 ft/hr model agrees relatively well with the observed values for most of the piezometer locations. The WB, WR, EB, and ER, piezometer locations are centered on the one-to-one fit line and the  $R^2$  value improves to 0.92. The ER and WR piezometer locations show the greatest improvement from the lower bulk hydraulic conductivity model cases. The WDE piezometer location values only improve marginally.

There is an apparent spatial relationship between the model fit and piezometer distance from the river. The closer piezometer locations form a thinner spatial pattern than piezometer further from the river. The ER piezometer for example, tightly fits the one to one line whereas the EDW and WDE piezometers are more scattered. The ER and WR locations show the greatest improvement from the lower bulk hydraulic conductivity models, whereas the WDE piezometer location only improves marginally.

It is also important to note that the number of overestimated and underestimated values is almost equal for the 15 ft/hr model scenario, which will affect averaging for all the model values. This is important to note because statistics like root mean squared error and mean absolute error will underestimate the average error, indicating a better model fit than is actually present.

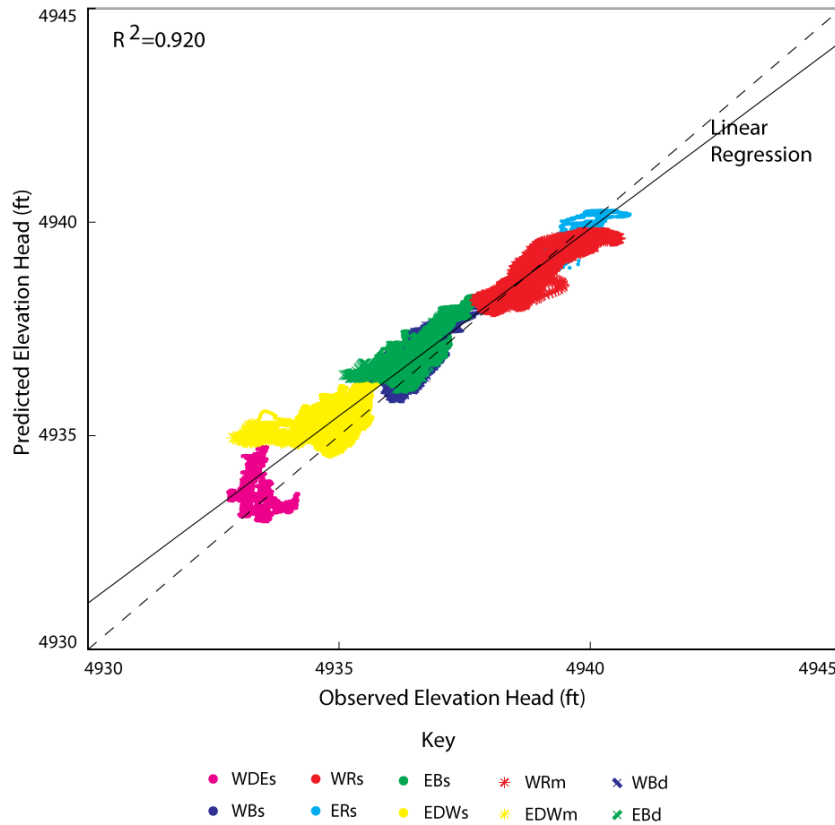


**Figure 8.12: Plot of predicted vs. observed values of water table elevation for 15 ft/hr homogenous subsurface model. ( $ss=3.048 \times 10^{-5} \text{ ft}^{-1}$ )**

Figure 8.13 is a scatterplot of the observed values and the layered subsurface Case 1 model case predicted values, where the shallow piezometers are represented by dots, the mid

piezometers by stars, the deep piezometers by xs, the one-to-one fit line by a dashed black line, and the linear regression line by a solid black line.

The Case 1 layered subsurface model case responds very similarly to the 15 ft/hr bulk hydraulic conductivity homogenous subsurface model. The layered subsurface model case agrees relatively well with the observed values for most of the piezometer locations. The WB, WR, EB, and ER, piezometer locations are centered on the one-to-one fit line and the  $R^2$  value for the linear regression is 0.92.

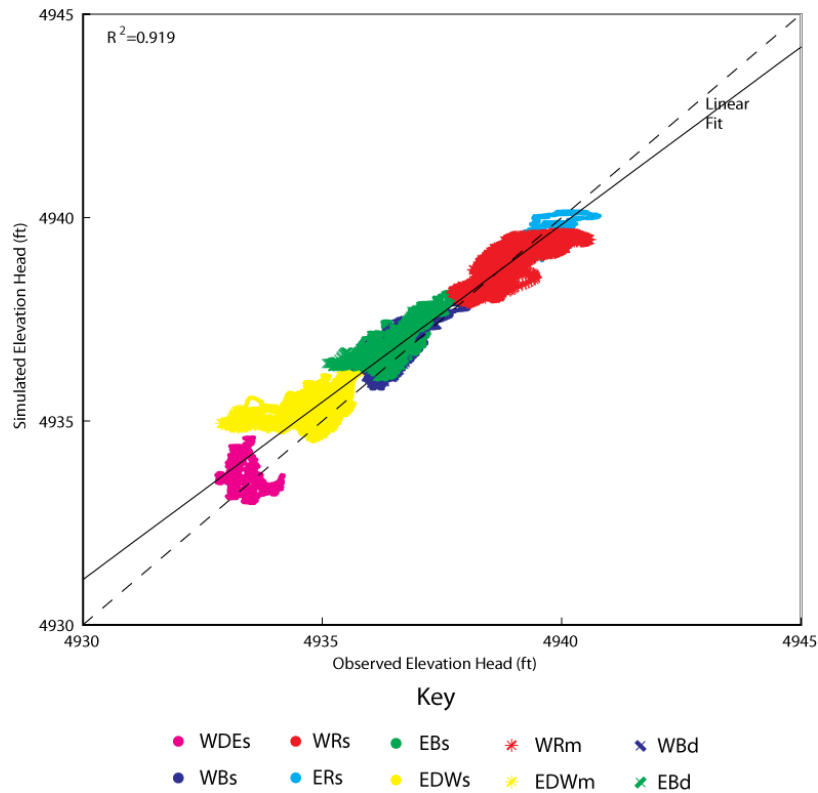


**Figure 8.13: Plot of predicted vs. observed values of water table elevation for Case 1 layered subsurface model. ( $ss=3.048 \times 10^{-5} \text{ ft}^{-1}$ )**

Figure 8.14 is a scatterplot of the observed values and the random field subsurface model case predicted values, where the shallow piezometers are represented by dots, the mid piezometers by stars, the deep piezometers by xs, the one-to-one fit line by a dashed black line, and the linear regression line by a solid black line.

The random field subsurface model case responds very similarly to the 15 ft/hr bulk hydraulic conductivity homogenous subsurface and Case 1 layered subsurface model cases. The random field subsurface model case predicted values agrees relatively well with the observed values for most of the piezometer locations. The WB, WR, EB, and ER, piezometer locations are centered on the one-to-one fit line and the  $R^2$  value for the linear regression is 0.92. The  $R^2$  values for the 15ft/hr homogenous subsurface model case, Case1 layered subsurface model case, and the random field model case indicates the three model scenarios provide an equal model fit.

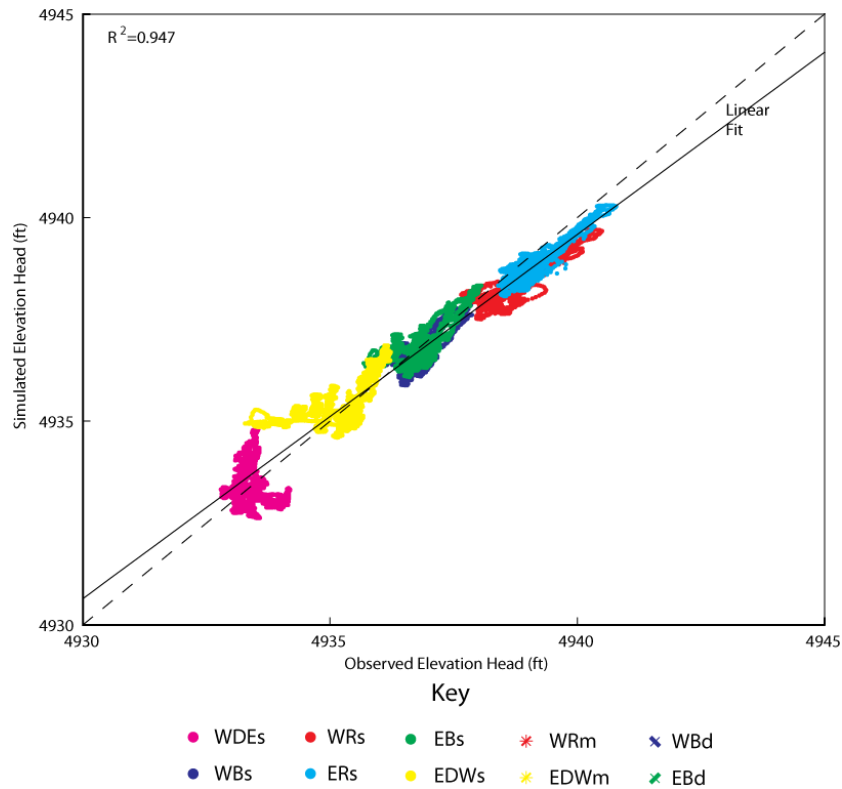


**Figure 8.14: Plot of predicted vs. observed values of water table elevation for random field subsurface model. ( $ss=3.048 \times 10^{-5} \text{ ft}^{-1}$ )**

#### 8.4 Index of agreement

The index of agreement was calculated for all of the numerical model scenarios and the results are presented in Table 8.10, 8.11, and 8.12. Index of agreement values range from zero to one, where higher values indicate better model fitness. The calculated index of agreement values for the homogenous subsurface model cases are presented in Table 8.10 and the values range from 0.14 to 0.96. Index of agreement values appear to correlate with bulk hydraulic conductivity

and proximity to the river. Based on the calculated index of agreement values, models using higher bulk hydraulic conductivity values (10, 15, 20 ft/hr) better fit the observed data. The WDEs piezometer is the only exception to this observation, but all homogenous subsurface model cases poorly fit the observed data.

As the distance between the river and piezometer increases, the model fit generally decreases. The best model fits are observed at the ERs piezometer (closest to the river) and the worst at the WDEs piezometer (furthest from the river). Relatively strong model fits are observed for all of the piezometer locations using the higher bulk hydraulic conductivity values, but the WDEs piezometer. When the bulk hydraulic conductivity value is held constant and the specific storage is varied, the index of agreement values remain relatively constant. This indicates that hydraulic conductivity is more influential to model fit than specific storage.

**Table 8.10: Index of agreement values for the homogenous subsurface model scenarios.**

Model Number	Hydraulic conductivity (ft/hr)	Specific Storage ( $ft^{-1}$ )	WDEs	WBs	ERs	WRm	EDWm	WBd	EBd
1	0.083	$3 \times 10^{-5}$	0.35	0.41	0.44	0.43	0.05	0.40	0.14
2	0.083	$3 \times 10^{-6}$	0.35	0.41	0.44	0.43	0.05	0.40	0.14
3	0.083	$3 \times 10^{-7}$	0.35	0.41	0.44	0.43	0.05	0.40	0.14
4	0.417	$3 \times 10^{-5}$	0.34	0.40	0.43	0.44	0.12	0.39	0.25
5	0.417	$3 \times 10^{-6}$	0.34	0.40	0.43	0.44	0.12	0.39	0.25
6	0.417	$3 \times 10^{-7}$	0.34	0.40	0.43	0.44	0.12	0.39	0.25
7	2.042	$3 \times 10^{-5}$	0.25	0.31	0.42	0.41	0.45	0.30	0.44
8	2.042	$3 \times 10^{-6}$	0.25	0.31	0.42	0.41	0.45	0.30	0.44
9	2.042	$3 \times 10^{-7}$	0.25	0.31	0.42	0.41	0.45	0.30	0.44
10	3.75	$3 \times 10^{-5}$	0.23	0.30	0.43	0.41	0.50	0.28	0.46
11	3.75	$3 \times 10^{-6}$	0.23	0.29	0.43	0.41	0.50	0.28	0.46
12	3.75	$3 \times 10^{-7}$	0.23	0.29	0.43	0.41	0.50	0.28	0.46
13	10	$3 \times 10^{-5}$	0.24	0.84	0.90	0.81	0.73	0.80	0.80
14	10	$3 \times 10^{-6}$	0.16	0.82	0.95	0.93	0.68	0.73	0.73
15	10	$3 \times 10^{-7}$	0.16	0.84	0.94	0.90	0.71	0.77	0.77
16	15	$3 \times 10^{-5}$	0.15	0.83	0.96	0.93	0.66	0.74	0.72
17	15	$3 \times 10^{-6}$	0.15	0.82	0.96	0.94	0.68	0.74	0.74
18	15	$3 \times 10^{-7}$	0.16	0.85	0.94	0.9	0.71	0.78	0.78
19	20	$3 \times 10^{-5}$	0.15	0.83	0.96	0.94	0.66	0.74	0.72
20	20	$3 \times 10^{-6}$	0.15	0.83	0.96	0.94	0.68	0.75	0.75
21	20	$3 \times 10^{-7}$	0.16	0.85	0.94	0.90	0.71	0.78	0.78

The calculated index of agreement values for the layered subsurface model cases are shown in Tables 8.11 and the values range from 0.16 to 0.95. The index of agreement values do not vary greatly for the Case 1, Case 2, and Case 4 layered subsurface modeling scenarios. Case 3 appears to better predict values at the WDEs piezometer, but provides a worse model fitness at the ERs and WRm piezometers. The layered subsurface models generally provide very similar results to the homogenous subsurface 15 ft/hr bulk hydraulic conductivity model cases.

**Table 8.11: Index of agreement values for the layered subsurface models.**

Model Number	Case Number	Specific Storage (ft <sup>-1</sup> )	WDEs	WBs	ERs	WRm	EDWm	WBd	EBd
22	Case 1	3.x10 <sup>-5</sup>	0.17	0.80	0.94	0.89	0.66	0.72	0.71
23	Case 1	3.x10 <sup>-6</sup>	0.18	0.84	0.92	0.85	0.72	0.77	0.78
24	Case 1	3.x10 <sup>-7</sup>	0.17	0.83	0.92	0.86	0.71	0.76	0.77
25	Case 2	3.x10 <sup>-5</sup>	0.16	0.81	0.94	0.91	0.66	0.73	0.72
26	Case 2	3.x10 <sup>-6</sup>	0.16	0.81	0.95	0.91	0.68	0.73	0.74
27	Case 2	3.x10 <sup>-7</sup>	0.18	0.84	0.91	0.85	0.73	0.79	0.79
28	Case 3	3.x10 <sup>-5</sup>	0.32	0.77	0.90	0.79	0.66	0.71	0.70
29	Case 3	3.x10 <sup>-6</sup>	0.32	0.78	0.90	0.79	0.68	0.71	0.73
30	Case 3	3.x10 <sup>-7</sup>	0.31	0.81	0.88	0.75	0.72	0.76	0.77
31	Case 4	3.x10 <sup>-5</sup>	0.17	0.80	0.93	0.88	0.66	0.71	0.71
32	Case 4	3.x10 <sup>-6</sup>	0.17	0.80	0.93	0.87	0.68	0.72	0.73
33	Case 4	3.x10 <sup>-7</sup>	0.18	0.81	0.92	0.86	0.70	0.74	0.75

The index of agreement values for the random field subsurface model cases are shown in Table 8.12 and values range from 0.14 to 0.96. The index of agreement values do not vary greatly between the different random field subsurface modeling scenarios and provide very similar results to the homogenous subsurface 15 ft/hr bulk hydraulic conductivity and layered subsurface model cases.

**Table 8.12: Index of agreement values for the random field subsurface models.**

Model Number	Specific Storage (ft <sup>-1</sup> )	WDEs	WBs	ERs	WRm	EDWm	WBd	EBd
34	3.x10 <sup>-5</sup>	0.14	0.84	0.96	0.95	0.66	0.75	0.73
35	3.x10 <sup>-6</sup>	0.15	0.83	0.96	0.96	0.68	0.74	0.74
36	3.x10 <sup>-7</sup>	0.15	0.85	0.95	0.93	0.71	0.78	0.78

## 8.5 Hydraulic Gradients

Horizontal and vertical hydraulic gradients were calculated at two locations for three numerical model cases: (1) the 15 ft/hr bulk hydraulic conductivity,  $3.048 \times 10^{-5} \text{ ft}^{-1}$  specific storage, homogenous subsurface model case (Model 16), (2) the Case 1,  $3.048 \times 10^{-5} \text{ ft}^{-1}$  specific storage, layered subsurface model case (Model 22), and (3) the  $3.048 \times 10^{-5} \text{ ft}^{-1}$  specific storage, random field subsurface model case (Model 34). Hydraulic gradients were calculated at two locations: location 1 is near the western bank of the Rio Grande and location 2 is below the center of the Rio Grande.

The average horizontal hydraulic gradients are presented in Table 8.13. The average horizontal gradients were similar between the three model cases at both locations and the standard deviation was small for all the model cases. The average numerical model horizontal hydraulic gradients were an order magnitude larger than the average horizontal gradients calculated for the Barelás Cross-section (eastside  $9.02 \times 10^{-3}$  and westside  $9.42 \times 10^{-3}$ ).

**Table 8.13: Comparison of Numerical Model Horizontal Gradients**

Location	Homogenous Subsurface		Layered Subsurface		Random Field Subsurface	
	Average	Standard Deviation	Average	Standard Deviation	Average	Standard Deviation
1	$8.66 \times 10^{-2}$	$5.57 \times 10^{-4}$	$8.10 \times 10^{-2}$	$5.20 \times 10^{-4}$	$4.28 \times 10^{-2}$	$1.28 \times 10^{-2}$
2	$5.10 \times 10^{-2}$	$8.40 \times 10^{-15}$	$5.10 \times 10^{-2}$	$8.40 \times 10^{-15}$	$5.83 \times 10^{-2}$	$2.20 \times 10^{-3}$

The average vertical hydraulic gradients are presented in Table 8.14. The average vertical gradients were similar between the compared model cases for both locations and the standard deviation was small. The average numerical model vertical hydraulic gradients were an order magnitude larger than average numerical model horizontal hydraulic gradients. This indicates vertical flow is more influential than horizontal flow near the river in all of the compared model cases.

**Table 8.14: Comparison of Numerical Model Vertical Gradients near Rio Grande**

Location	Homogenous Subsurface		Layered Subsurface		Random Field Subsurface	
	Average	Standard Deviation	Average	Standard Deviation	Average	Standard Deviation
1	$3.49 \times 10^{-1}$	$2.30 \times 10^{-3}$	$4.24 \times 10^{-1}$	$3.55 \times 10^{-3}$	$7.23 \times 10^{-1}$	$1.03 \times 10^{-1}$
2	$6.47 \times 10^{-1}$	$3.02 \times 10^{-5}$	$6.50 \times 10^{-1}$	$5.80 \times 10^{-4}$	$7.24 \times 10^{-1}$	$1.99 \times 10^{-2}$

**8.6 Fourier Transforms**

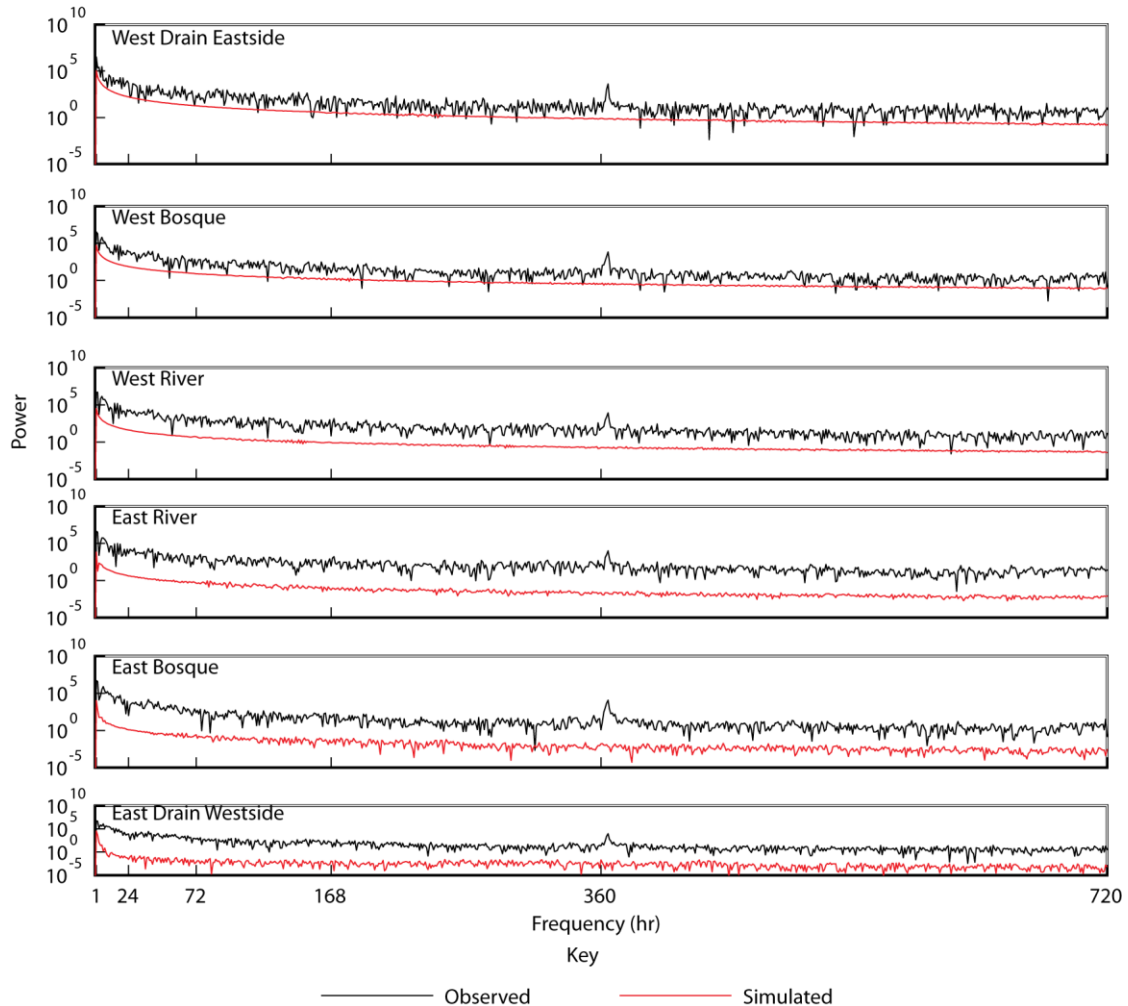
Fourier transforms were performed for all of the model cases. Figure 8.15 shows the 0.417 ft/hr bulk hydraulic conductivity,  $3.048 \times 10^{-5} \text{ ft}^{-1}$  specific storage, homogenous subsurface model results for the shallow piezometer locations. Here, the observed values are represented by a black solid line and the predicted values by a red solid line.

Figure 8.15 shows the observed values have their strongest power at short frequencies, 24 hours or less. This indicates changes in pressure throughout the aquifer rapidly equilibrate. After the 24 hour (1 day) frequency, the observed value's power steadily decreases.

Figure 8.15 also shows the 0.417 ft/hr homogenous subsurface model case predicted Fourier Transform values do not agree well with the observed Fourier Transform values. The 0.417 ft/hr homogenous subsurface model does not predict the frequency or amplitude of the observed values. The numerical model does predict a stronger power for the one-hour frequency, but it does not predict stronger powers at the other time frequencies displayed by the observed values. This indicates that the 0.417 ft/hr homogenous subsurface model case would not be able to effectively predict most of the characteristic times observed at the Barelás cross-section.

Figure 8.16 shows the 15 ft/hr bulk hydraulic conductivity,  $3.048 \times 10^{-5} \text{ ft}^{-1}$  specific storage, homogenous subsurface model results for the shallow piezometer locations, where the observed values are represented by a black solid line and the predicted values by a red solid line. The observed and predicted Fourier Transform values agree reasonably well for this case. The power predicted by the model is of the same order of magnitude (amplitude) as the observed values. Similarly to the other numerical model results, there appears to be a spatial relationship for model fitness. The WB, EB, and EDW piezometer locations' predicted values appear to better fit the observed values. The 15 ft/hr homogenous subsurface model case better predicts the

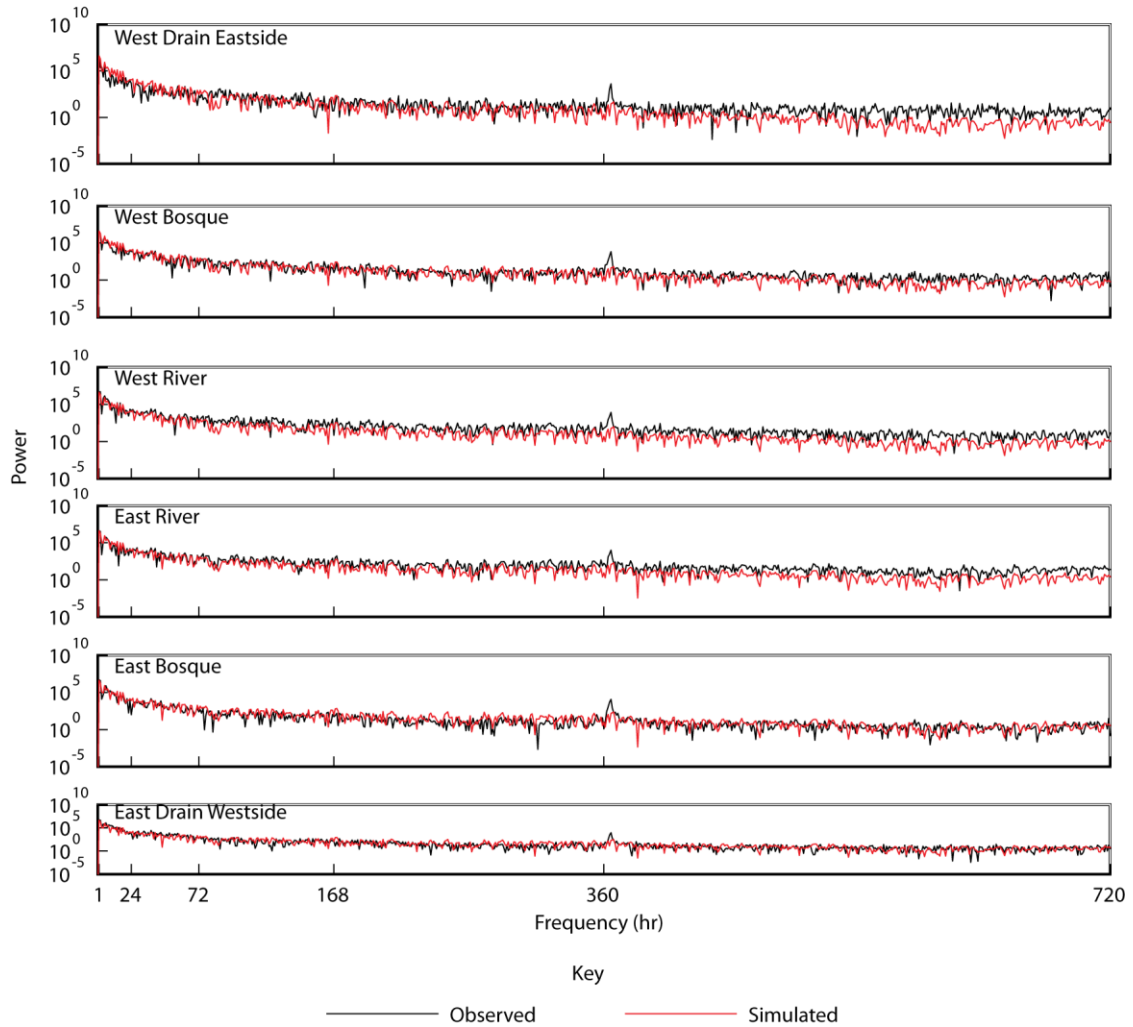
frequency or amplitude of the observed values than the 0.417 ft homogenous subsurface model case.



**Figure 8.15: Fourier transforms for the 0.417 ft/hr bulk hydraulic conductivity model. Shallow piezometer locations are shown here.**

Figure 8.17 shows the 15 ft/hr bulk hydraulic conductivity,  $3.048 \times 10^{-5} \text{ ft}^{-1}$  specific storage, homogenous subsurface model results for the mid piezometer locations, where the observed values are represented by a black solid line and the predicted values by a red solid line. The observed and predicted Fourier Transform values have the same trends at mid piezometer depth. The power predicted by the numerical model is of the same order of magnitude as the observed values. The numerical model predicted values appear to be underestimated for the longer frequencies at the WR piezometer location, whereas the predicted values at EDW

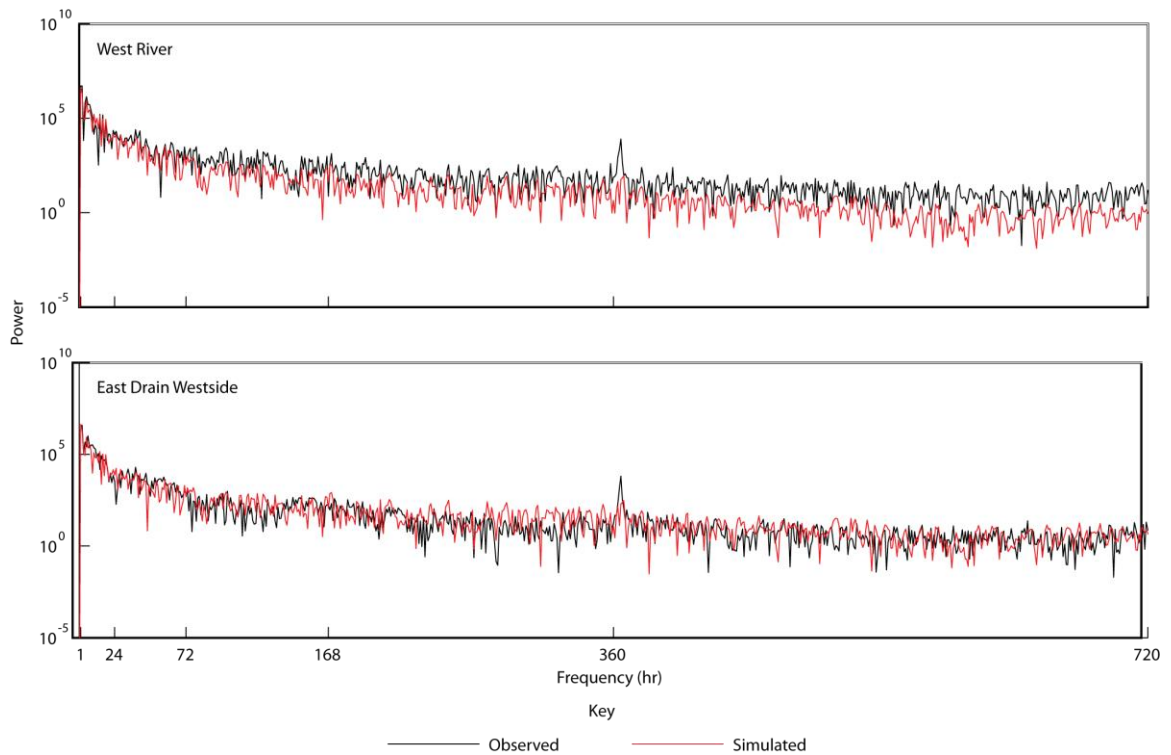
piezometer location do not appear to be consistently over or under estimated.



**Figure 8.16: Fourier transforms for the 15ft/hr bulk hydraulic conductivity homogenous subsurface model. Shallow piezometer locations are shown here.**

Figure 8.18 shows the 15 ft/hr bulk hydraulic conductivity,  $3.048 \times 10^{-5} \text{ ft}^{-1}$  specific storage, homogenous subsurface model results for the deep piezometer locations, where the observed values are represented by a black solid line and the predicted values by a red solid line. The deep piezometer response is similar to the mid piezometer response. Like the shallow and mid piezometers, the power predicted by the numerical model for the deep piezometers is of the same order of magnitude as the observed values. The strongest power is observed at frequencies less than 24 hours.

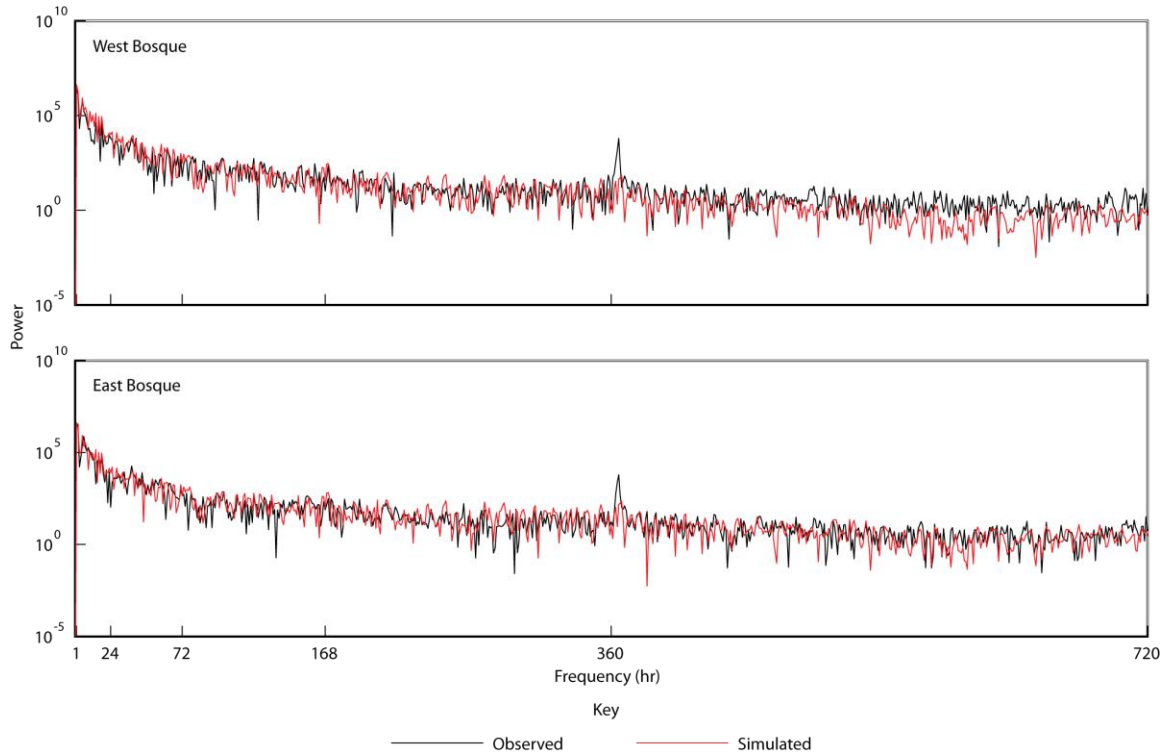
Figure 8.19 shows the Case 1,  $3.048 \times 10^{-5} \text{ ft}^{-1}$  specific storage, layered subsurface model results for the shallow piezometer locations, where the observed values are represented by a black solid line and the predicted values by a red solid line. The observed and predicted Fourier Transform values agree reasonably well for this case. The Case 1 layered subsurface model responds similarly to the 15 ft/hr bulk hydraulic conductivity homogenous subsurface model for all piezometer locations. Like the 15 ft/hr homogenous subsurface model case, the Case 1 layered subsurface model case results show model fitness to be related to the piezometer's distance from the river. The WB, EB, and EDW piezometer locations' predicted values appear to better fit the observed values than predicted values for the other piezometer locations.



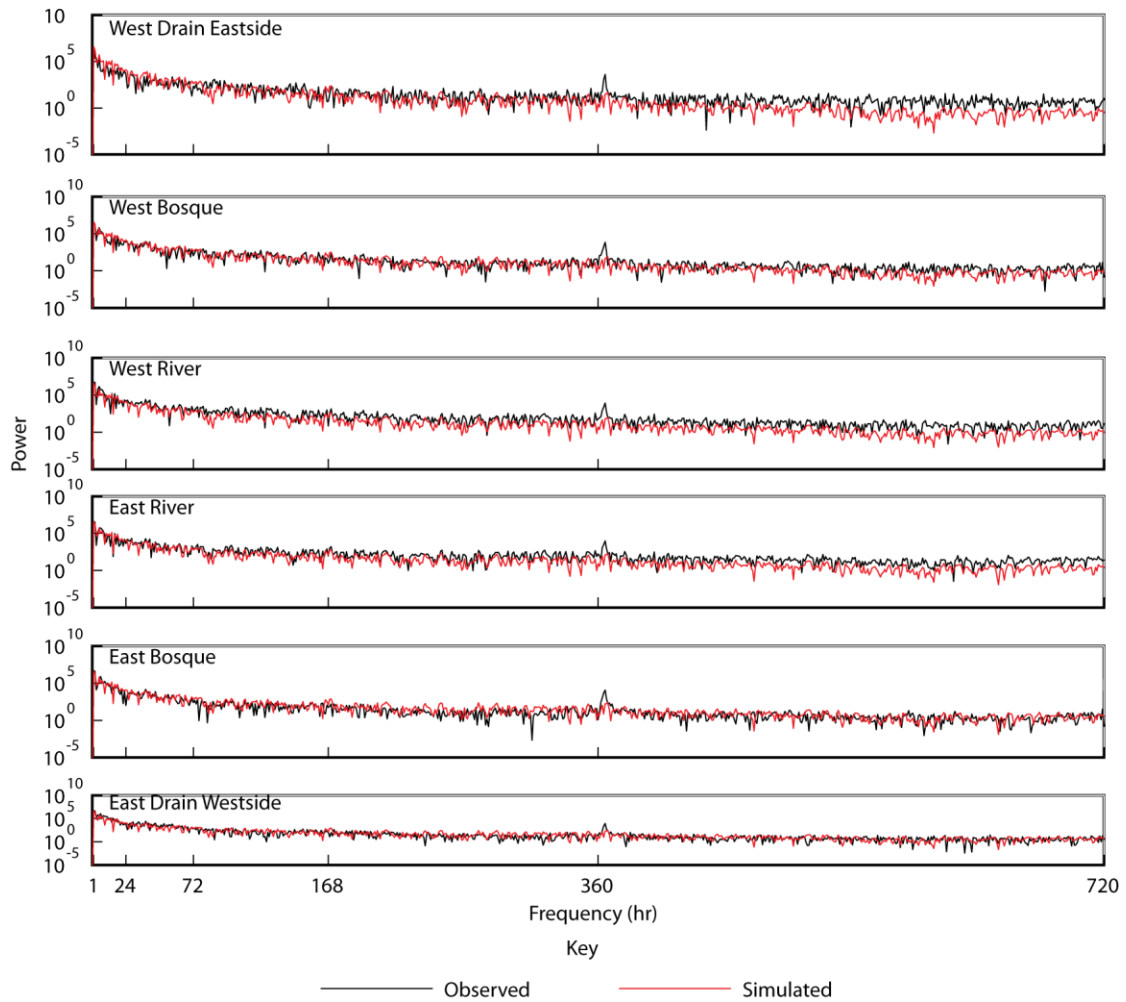
**Figure 8.17: Fourier transforms for the 15ft/hr bulk hydraulic conductivity homogenous subsurface model. Mid piezometer locations are shown here.**

Figure 8.20 shows the  $3.048 \times 10^{-5} \text{ ft}^{-1}$  specific storage, random field subsurface model results for the shallow piezometer locations, where the observed values are represented by a black solid line and the predicted values by a red solid line. The observed and predicted Fourier Transform values agree reasonably well for this case. The power predicted by the numerical model is of the same order of magnitude as the observed values. The random field subsurface

model responds similarly to the 15 ft/hr bulk hydraulic conductivity homogenous subsurface and Case 1 layered subsurface model for all piezometer locations. However, the random field subsurface model case better predicts the power of the longer frequencies than the homogenous subsurface and layered subsurface cases. This suggests that improved subsurface characterization improves the prediction of longer characteristic times for Barelas Cross-section.



**Figure 8.18: Fourier transforms for the 15 ft/hr bulk hydraulic conductivity homogenous subsurface model. Deep piezometer locations are shown here.**



**Figure 8.19: Fourier transforms for the Case 1 layered subsurface model. Shallow piezometer locations are shown here.**

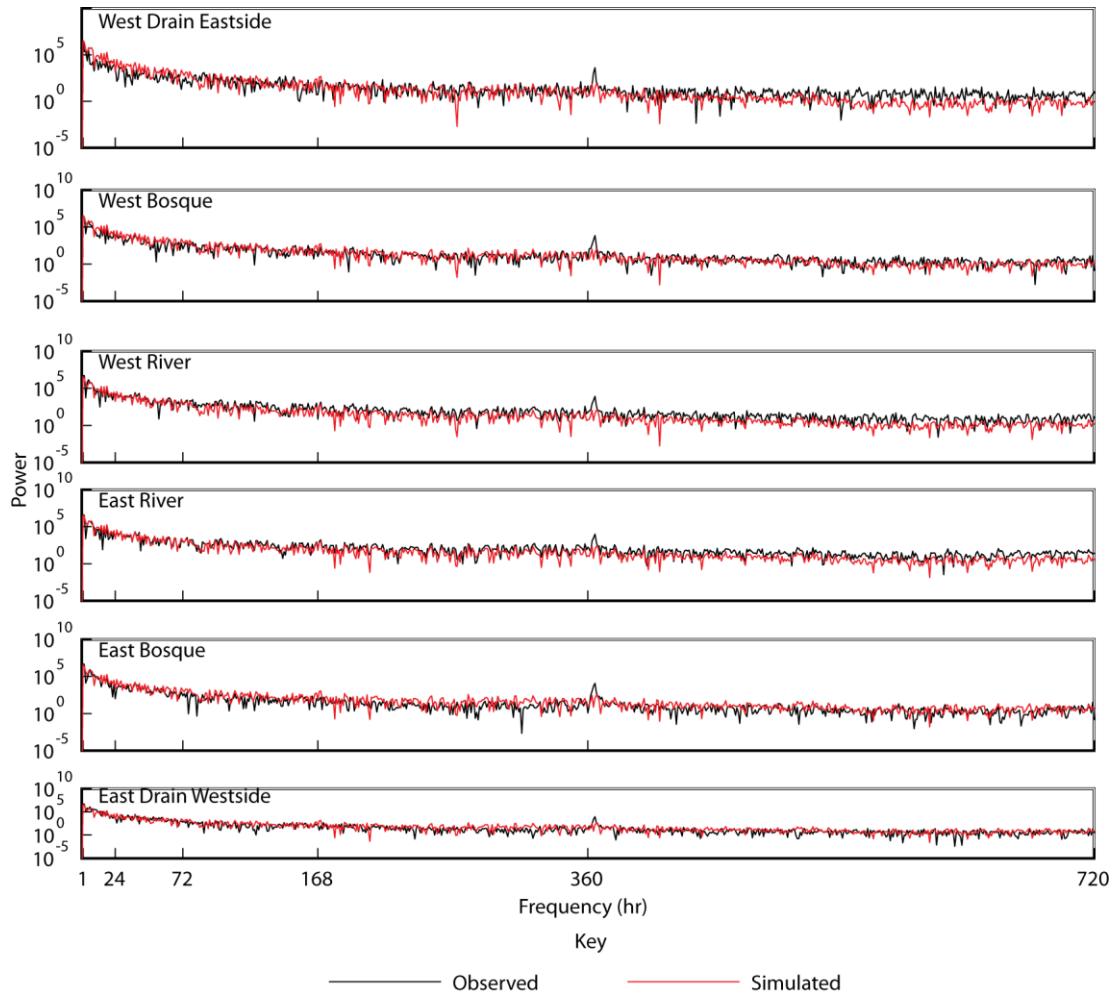


**Figure 8.20: Fourier transforms for the random field subsurface model. Shallow piezometer locations shown here.**

## CHAPTER 9: DISCUSSION AND CONCLUSIONS

The goal of this research was to quantify the interactions between the Santa Fe Aquifer Group and the Rio Grande using a combination of observations, analytical modeling, and numerical modeling.

A graphical analysis of the observed data revealed several spatial and temporal relationships for the Barelás Cross-section:

- 1) Water table elevation at all of the piezometer locations raised and lowered correspondingly with the Rio Grande river stage raising and lowering. This suggests strong connectivity between the Santa Fe Group Aquifer and the Rio Grande.
- 2) As the distance between the river and piezometer (observation point) increases the more dampened and lagged the pressure signal created by the Rio Grande becomes. Thus the water level signal at piezometer nests closer to the river look more similar to the river signal than the water level signal at piezometer nests further from the river.
- 3) As the piezometer depth increases the pressure signal created by the Rio Grande becomes more dampened and lagged. Thus the water level signal at the shallow piezometers looks more similar to the river signal than the water level signal at deeper piezometers.
- 4) Two seasonal trends were observed for the Rio Grande: (1) peak flow in the Rio Grande occurred between April and June, which corresponds to the annual spring runoff period in this region and (2) frequent, small peaks occurred between July and September, which corresponds to the summer monsoon period in this region.

River leakage or Darcy flux was calculated for each of the Middle Rio Grande Valley Monitoring network cross-section locations. Several key observations have been made:

- 1) The average cross-section hydraulic conductivity ranges from 39 ft/day at the Barelás and Pajarito cross-sections to 140 ft/day at the Central cross-section. The average hydraulic conductivity at the Barelás cross-section was 41 ft/day.
- 2) Average horizontal hydraulic conductivity values ranged from  $2.54 \times 10^{-3}$  at the Interstate 25 Eastside to  $1.53 \times 10^{-2}$  at the Alameda Eastside. The averaged horizontal hydraulic gradient values vary from cross-section to cross-section, but also vary as a

much as an order of magnitude within a cross-section. The horizontal hydraulic gradients at Barelás cross-section are relatively.

- 3) The average Darcy flux values ranged from 0.04 feet per day (ft/day) at the Montano Westside to 1.12 ft/day at the Central Eastside. Values vary from cross-section to cross-section, but also within the cross-section between eastside and westside of the river.

Three analytical models were performed for the 2006-2007 water year. An analysis of model fitness was performed, which included calculating the average, standard deviation, and index of agreement for each analytical model scenario at each piezometer location. Overall, the index of agreement results indicated the transient analytical models did a poor job of predicting the observed values.

Thirty-six ParFlow model scenarios were simulated for the 2006-2007 water year. An analysis of model fitness was performed each of the model scenarios, which included: calculating the average and standard deviation for each piezometer for all of the model scenarios, graphically comparing different model scenarios, plotting the observed values against the numerical model predicted values and calculating an  $R^2$  value for each model scenario, calculating an index of agreement value for each piezometer location for all of the model scenarios, calculating horizontal and vertical gradients for a subset of the model cases, and performing Fourier Transform on the observed values and the numerical model predicted values for each model scenario. Several key observations have been made from this analysis.

- 1) The average and standard deviation results show that increasing the variability in the model subsurface representation does not significantly change the calculated average water table elevation. However, it does increase in the standard deviation.
- 2) Overall the numerical modeling results demonstrated that as distance between the piezometer and the river increases, piezometer signal is dampened and lagged. As piezometer depth increases, piezometer signal is dampened and lagged.
- 3) Hydraulic conductivity and specific storage play very different roles in the model results. Hydraulic conductivity is directly related to model goodness of fit. Low hydraulic conductivity values result in weak model fits, whereas higher values predict better model fits. Specific storage is directly related to how many of the high

frequency river signal changes are predicted by the numerical model at the piezometer locations.

- 4) Differing model scenarios (i.e. through different subsurface characterizations) provide an equally “good” model fit. The higher bulk hydraulic conductivity homogenous subsurface models (10, 15, and 20 ft/hr), layered subsurface models, and the random field subsurface models all provided quantitatively similar results using a suite of standard measures of performance. This suggests that the pressure observations depend more strongly on effective parameters than on local heterogeneities in hydraulic conductivities.
- 5) Model scenarios using higher hydraulic conductivity values predicted better fits to the observed Fourier transform values—indicating a better representation of the critical times for this system. The predicted values for the deeper piezometers showed a slight lag from the observed values, but still maintained the observed values trends. The 15 ft/hr bulk hydraulic conductivity homogenous subsurface, layered subsurface, and random field subsurface models produced similar predicted values. .
- 6) The numerical model results strongly indicate the average hydraulic conductivities calculated for the study area using the Bouwer and Rice (1976) and the Bulter (1998) slug-test analysis methods for unconfined aquifers are underestimation of the average hydraulic conductivities for the Barelàs cross-section.
- 7) The numerical model results suggest the average horizontal hydraulic gradients calculated for the study area using an adaptation on the three-point method and the daily-mean groundwater levels are underestimation for the Barelàs cross-section.

The findings of this study are limited by the following factors:

1) The USGS collected the data used in this study by a variety of techniques with varying degrees of uncertainty. For example, the slug tests method used to determine the range of hydraulic conductivity values used in the ParFlow models are known to have high uncertainty associated with them.

2) Limited information was collected to characterize the extent and nature of subsurface heterogeneity for the study area.

3) The graphical analysis showed hourly, seasonally, and yearly variation in the river and piezometer signals. Five years of data have been collected for the study area, but only one water year was analyzed for the 36 model scenarios. In order to better understand groundwater-surface water interaction within the study area, a longer period should be analyzed for the model scenarios.

## REFERENCES

- Alley, W.M., Healy, R.W., LaBaugh, J. W., and Reilly, T.E, 2002, Flow and storage in groundwater systems, *Science*, v. 296, 1985-1990 p.
- Anderson, M.P., Woessner, W.W., 2002. Applied groundwater modeling simulation of flow and advective transport: Academic Press, San Diego, CA, 381 p.
- Ashby, S.F. and Falgout, R.D. 1996. A parallel multigrid preconditioned conjugate gradient algorithm for groundwater flow simulations. *Nuclear Science and Engineering*. 124. 145-159 p.
- Bartilino, J.R. and J.C. Cole, 2002, Ground-Water Resources of the Middle Rio Grande Basin, New Mexico, U.S. Geological Survey Circular 1222. 132p.
- Bexfield, L.M and D.P. McAda, 2003, Simulated effects of groundwater management scenarios on the Santa Fe Group aquifer system, Middle Rio Grande Basin, New Mexico, 2001-40: U.S. Geological Survey Water-Resources Investigations Report 03-4040, 39p.
- Bouwer, Herman, and Rice, R.C., 1976, A slug test for determining hydraulic conductivity of unconfined aquifers with completely or partially penetrating wells: *Water Resources Research*, v. 12, no. 3, 423-428 p.
- Brutsaert, W., 2005, *Hydrology an introduction*: Cambridge University Press, New York, 605 p.
- Butler, J.J., 1998, *The design, performance, and analysis of slug tests*: Lewis Publishers, Boca Raton, Florida, 252 p.
- Butler, J.J., Zlotnik, V. A., and Tsou, M.S., 2001, Drawdown and stream depletion produced by pumping in the vicinity of a partially penetrating stream, *Groundwater*, v. 39, no. 5, 651-658 p.
- Christensen, S., Zlotnik, V.A., Tartakovsky, D.M., 2009. Optimal design for pumping tests in leaky aquifers for stream depletion analysis, *Journal of Hydrology*, v. 375, 554-565 p.
- Cohen, R., 2011, *Surface water quality modeling: lecture 7 Lake modeling*, slide 14.

- Compton, Robert R., 1962, Manual of field geology: John Wiley and Sons, Inc, New York, 31 p.
- Dingman, S.L., 2002, Physical hydrology 2<sup>nd</sup> ed.: Prentice Hall: Upper Saddle River, NJ, 646 p.
- DHI-WASY Software, 2012, FEFLOW 6.1: Finite element subsurface flow & transport simulation system, Berlin, Germany, p.
- Fetter, C.W., 2001, Applied Hydrogeology 4<sup>th</sup> ed.: Prentice-Hall, Upper Saddle River, NJ, 81-82 and 164-165 p.
- Harbaugh, A.W., Banta, E.R., Hill, M.C., and M.G. McDonald, 2000, MODLFOW-2000, The U.S. Geological survey modular ground-water model-user guide to modularization concepts and the groundwater-flow process, Open-File Report 00-92.
- Hawley, J.W. and Haase, C.S., 1992, Hydrogeologic framework of the northern Albuquerque Basin: Socorro, New Mexico Bureau of Mines and Mineral Resources, Open-File Report 387, 176p.
- Hunt, B., 1999, Unsteady stream depletion from ground water pumping, Ground Water, v. 37, no. 1, 98-102 p.
- Jones, J.E. and C.S. Woodward. 2001. Newton-krylov-multigrid solvers for large scale, highly heterogeneous variably saturated flow problems. Advances in Water Resources. 24. 763-774 p.
- Kirchner, J. W., Feng, X., Neal, C., and A. J. Robson, 2004, The fine structure of water-quality dynamics: the (high-frequency) wave of the future, Hydrologic Processes, v. 18, 1353-1359 p.
- Kollet, S.J. and V.A. Zlotnik, 2003, Stream depletion predictions using pumping test data from a heterogeneous stream-aquifer system (a case study from the Great Plains, USA), Journal of Hydrology, v. 281, 96-114 p.
- Kollet, S.J. and V.A. Zlotnik, 2007, Evaluation of the streambed leakage concept in analytical models using data from three pumping tests. Hydrogeology Journal, v. 15, 1051-1062 p.

- Maxwell, R.M., Kollet, S.J., Smith, S.G, Woodward, C.S., Falgout, R.D., Ferguson, I.M, Baldwin, C. Bosl, W.J., Hornung, R., Ashby, S., 2010, ParFlow User's manual. International Groundwater Modeling, Center Report GWMI 2010-01, 132p.
- McAda, D.P., 1996, Plan of study to quantify the hydrogeologic relations between the Rio Grande and the Santa Fe Group aquifer system near Albuquerque, Central New Mexico: U.S. Geologic Survey Water Resources Investigations Report 96-4006.
- McAda, D.P., 2002. Simulation of groundwater flow in the middle Rio Grande Basin between Cochiti and San Acacia, New Mexico: U.S. Geological Survey Water Resources Investigations Report 02-4200.
- Myers, N.C., Finnegan, P.J., and Breedlove, J.D., 1999, Analysis of water-level data and groundwater flow modeling at Fort Riley, Kansas: U.S. Geological Survey Water-Resources Investigations Report 99-4115, 6 p.
- Plummer, L.N., Bexifield, L.M., Anderholm, S.K., Sanford, W.E., and Busenberg, E. 2004. Hydrochemical tracers in the middle Rio Grande Basin, USA: 1. Conceptualization of groundwater flow. *Hydrogeology Journal*. 12. 359-388 p.
- Rankin, D., McCoy, K., Moret, G., Worthington, J., and Bandy-Baldwin, K. 2011. Groundwater Hydrology and Estimation of Horizontal Groundwater Flux from the Rio Grande at Selected Locations in Albuquerque, New Mexico, 2003-09. USGS Scientific Investigations Report. In review.
- Russell, L., Snelson, S, 1994, Structure and tectonics of the Albuquerque basin segment of the Rio Grande Rift: Insights from reflection seismic data, Special papers (Geological Society of America), 83–112 p.
- Serrano, S.E., and S. R. Workman, 1998, Modeling transient stream/aquifer interaction with the non-linear Boussinesq equation and its analytical solution, *Journal of Hydrology*, v. 206, 245-255 p.

- Sophocleous, M., 2002, Interactions between groundwater and surface water: the state of the science, *Hydrogeology Journal*, v.10, 52-67 p.
- Spanoudaki, K., Nanou-Giannarou, A., Paschalinos, Y., Memos, C.D., Stamou, A.I., 2010, Analytical Solutions to the Stream-Aquifer Interaction Problem: A Critical Review, *Global Nest Journal*, v. 12. 126-139 p.
- Stark, O.D.L., 1989, *Groundwater Mechanics*, Prentice Hall Inc., Englewood Cliffs, NJ, 19-86 p.
- Storey, B.D., Computing Fourier /series and Power Spectrum with MATLAB,TEX Paper, [faculty.olin.edu/bstorey/Notes/Fourier.pdf](http://faculty.olin.edu/bstorey/Notes/Fourier.pdf). October 25, 2012, 1-13 p.
- Thompson, A.F., Ababou, R., and Gelhar, L.W. 1989. Implementation of the three-dimensional turning bands random field generator. *Water Resources Research*. 25: 2227-2243 p.
- Willmont, C. J., 1982,Some comments on the Evaluation of Model Performance, *Bulletin of Meteorological Society*, 1309-1313 p.